Star-formation activity in Abell 2670

Floris Lugt

June 24 2003

Abstract

I present an analysis of the star-formation activity in cluster Abell 2670, detected using radio continuum observations at 20 cm. 46 Star-forming galaxies have been found. This unusually high level of activity can for a large part be explained by the fact that three subclusters are merging in A2670, where galaxies that have just passed the shock front of their subcluster start interacting with the ICM. Also galaxies at high density in the X-ray region have been found forming stars.
This result has been compared with the results of the spectral classification performed on galaxies. It is concluded that both the optical and the radio method to identify star-formation galaxies are not sufficient. Due to heavy dust extinction the blue colour and emission lines may not be visible in the optical observations, resulting in a false classification. Galaxies that have very recently started forming stars may not have produced sufficient Supernovae to result in a high radio flux, which makes those galaxies difficult to observe in the radio. When one wishes to get a complete picture of the star-forming activity, both methods should be pursued. A complete picture of the star-forming activity in Abell 2670 has been obtained in that way.

Preface

This project was done as a "groot onderzoek" as part of the fourth year of the Astronomy curriculum. The majority of the work has been done at Columbia University in New York, under supervision of Prof. J.H. van Gorkom.

Contents

1 Introduction

In 1980 Alan Dressler wrote a paper in which he described what is now known and accepted as the morphology-density relation (Dressler 1980). This relation states that there is an increase in the fraction of elliptical and S0 galaxies in regions of high surface density (like in clusters of galaxies) and an increase in the fraction of spiral galaxies in regions of lower surface density (as in the field) (Dressler 1980). The question then was, is this relation the result of a relation between the formation of galaxies and their environment, or is it an evolutionary effect; do spiral galaxies transform into S0 galaxies (as Spitze & Baade had already suggested thirty years earlier) and maybe even into ellipticals? The observation that the number of spirals in cluster cores is higher near z $\sim$ 0.5 than near z $\sim$ 0 and that the reverse is true for S0 galaxies (Dressler 1997), seems to indicate that there is at least one form of evolution that galaxies undergo when they fall into the center of a cluster.
Meanwhile, Butcher & Oemler were the first to notice the fact that there is an increase in the fraction of blue galaxies in the cores of rich and compact concentrated clusters with increasing redshift (Butcher & Oemler 1978, 1984). According to their measurements the fraction of blue galaxies is $\backsim$ 0.03 at z $\lesssim$ 0.01 and rises to $\backsim$ 0.25 at z $\sim$ 0.5. It is now known that at z $\backsim$ 1 the fraction even rises to $\backsim$ 0.8 (Rakos & Schombert 1995), so this Butcher-Oemler effect is a real and accepted phenomenon. Thanks to the Butcher-Oemler effect it is clear that there is an evolution of galaxies in clusters, at least in their colour. But what is the cause of this effect? Does it mean that at low redshift there are less young (i.e blue) stars, in other words is the star formation suppressed as galaxies fall into the cores of a cluster?
The statements of the Morphology-Density relation and the Butcher-Oemler effect have defined the discussion about the evolution of galaxies in clusters in the past 20 years. The Butcher-Oemler effect can possibly be explained for a substantial part by a decline in star-formation activity in galaxies. It is therefore useful to study the star-formation properties of galaxies throughout clusters. This will be the focus of this report.

1.1 Star-formation studied in the optical

The question is, why would the star-formation activity of galaxies in clusters of galaxies at higher z be greater than at lower z, resulting in a larger fraction of blue galaxies and hence the Butcher-Oemler effect? Due to certain processes in clusters galaxies must be losing their gas, which causes the star formation to be suppressed. Candidates for these processes are ram-pressure stripping, tidal forces, galaxy-galaxy interactions, mergers of galaxies, evaporation, or maybe some other process. To find out which one is or which ones are responsible, it is very interesting to look at the star-formation properties of galaxies throughout clusters themselves.
One way of looking at the star-formation properties, is by examining the spectral properties of single galaxies. Several spectroscopic studies have been made in the past and in 1987 Couch & Sharples were the first to make an attempt for a theory for an evolution-

ary process of the spectral populations in clusters. In this theory star-forming galaxies would go into a star-bursting phase while falling into a cluster, then the star-formation would be suppressed and a phase with little to no star-forming activity would be entered (the "post-starburst" phase), and finally galaxies would end up in a totally passive phase with no star-formation left at all. This followed the observation of Dressler & Gunn in 1983 of galaxies in a post-starburst phase, which can be recognized by having very few or no emission lines (mainly [OII] and Hα, meaning very few or no star-formation), but on the other hand strong Balmer absorption lines, indicating the presence of young stars. An evolutionary cycle with a starbursting phase therefore seemed to make sense, but the physical processes responsible for this cycle were not found.
The largest study which is done so far on the star-formation activity of galaxies in clusters, was done by the "MORPHS" collaboration (see e.g. Smail et al. 1997 and Dressler et al. 1997). They looked at the morphologies of magnitude-limited samples of galaxies of 10 rich clusters in the redshift range of $0.37 \leq z \leq 0.56$, using the Hubble Space Telescope. In the meantime they also performed a spectroscopic study of the same clusters, in order to determine the star-formation activity alongside the morphology for every galaxy in the sample (Dressler et al. 1999, Poggianti et al. 1999). Below I will briefly give the characteristics and the properties according to the results of the MORPHS collaboration, for every spectral class that they used and that I will use in this report. The classifications are based on equivalent widths of the [OII] 3727 Å emission line, which indicates the formation of stars, and the Hδ 4104 Å Balmer absorption line, coming mainly from young blue (A) stars. See also Table 1 for the characteristics of the spectral classes.

The k-class: Passive galaxies which show no signs of star-formation (which would be indicated by [OII] emission lines) or any young stars (which would be visible through Balmer absorption lines (Hδ)). They are dominated by elliptical and S0 galaxies, but also Sa and even later-type galaxies can be found in this class. They mostly reside in the cores of clusters and have red colours.
The k+a/a+k-class: k+a/a+k galaxies have little or no [OII] emission lines, but they do have Hδ absorption lines, the k+a class with equivalent width of 3 to 8 Å and the a+k class with more than 8 Å equivalent width. This indicates that there is no star-formation activity (anymore), but the galaxies do contain young A stars which must have been formed in the recent ($\lesssim$1.5 Gyr) past, since such massive stars do not live any longer than approximately that period of time. Especially the a+k class which is defined by strong Balmer lines must have been forming a lot of stars, which is why the k+a/a+k spectra are identified with post-starburst galaxies.
k+a Galaxies were found to be either ellipticals or spirals (or S0's) but mostly spirals, while all the a+k galaxies in the sample were S0's or spirals, although not many of these were found at all. Like the k galaxies, the k+a galaxies are red, while a+k galaxies can be somewhat bluer. Both classes reside in the cores of clusters but also outside the cores.
The k(e)-class: These are early spiral-like galaxies with hints of [OII] emission lines but little to no Balmer lines (Poggianti & van Gorkom 2001).
The e(c)-class: e(c) Galaxies are star-forming galaxies. Their spectra show both weak to moderate (equivalent width between 5 and 40 Å) [OII] emission lines as weak to

moderate Hδ absorption lines (EW <4 Å) and they are spiral galaxies. Most of them can be found in the field or in the cluster outside the center. Their colours range from blue to red but are usually blue.
The e(b)-class: This class contains galaxies with very strong [OII] emission lines (EW[OII] > 40 $\AA$), not minding the Balmer absorption lines which can have any strength. The strong emission indicates very strong star formation and therefore these galaxies are called starbursting galaxies. They are late-type spirals or irregulars and are very blue indeed. It is thought that the starbursting phase does not last very long ($\sim$ a few times 10^8 yr, the life-time of massive stars (Morrison & Owen, 2003)). They are very blue.
The e(a)-class: The galaxies with strong Balmer lines (EW Hδ > 4Å) and moderate to strong [OII] lines (EW[OII] > 5 Å) fall into the e(a) class. The difference with the e(c) class is that the Balmer line is strong and the difference with the e(b) class is that EW[OII] can be less than 40. When a galaxy has EW H$\delta > 4$ and EW[OII] > 40, then it can both fall into the e(b) class and into the e(a) class. Using another emission line indicative of star formation, Hα, to calculate the Star Formation Rate (SFR), one gets a 2 to 3 times higher result than when one uses the usual [OII]. It is therefore believed that e(a) galaxies are in fact starbursting, but generally with low EW[OII] due to extinction by dust, since Hα lines are less affected by dust. e(a) Galaxies are therefore called dusty starburtsts. Note that the difference between the e(a) and the k+a/a+k class is only the presence of [OII]. It is possible however, that due to extreme dust obscuration the [OII] emission is not visible and the galaxy is classified as k+a/a+k, but is in fact forming stars.
Because of the extinction they are generally not as blue as the e(b)'s, but still bluer than other types. The class contains spirals and irregulars.

The results are consistent with the evolutionary idea of galaxies that are stimulated to form stars as they fall into a cluster (this is suggested by the observation that a similar fraction of e(a) galaxies is found in the cluster as in the field, while in the cluster the fraction is diluted by the large passive population; no definitive conclusion has been given yet though), before this star-formation is extinguished as the galaxies get near to the center (i.e. near high density). The physical mechanisms that cause this evolution still have to be identified.
So the star-formation properties of galaxies in clusters of galaxies has been extensively looked at at intermediate redshift. For comparison of the results and to learn how the evolution continues and which processes are responsible for this evolution, the star-formation properties of clusters at low redshift needs to be looked at next. At the moment, van Gorkom and collaborators are doing an HI/optical study of 20 clusters out to a redshift of 0.2. One of these clusters is Abell 2670 at z $\sim$ 0.08.

Type	EW [OII] (Å)	EW Hδ (Å)	Notes
k	absent	< 3	passive elliptical-like
k+a	absent	3-8	post-starburst/star-forming
a+k	absent	> 8	as k+a, but stronger Hδ
k(e)	weak	< 4	early spiral-like, some [OII]
e(c)	> 5 and < 40	< 4	spiral-like, star-forming
e(a)	> 5	> 4	post-starburst, some star-formation
e(b)	> 40	any	starbursting
e	present	?	S/N too low to classify

Table 1. Spectral classification of galaxies (Dressler et al. 1999, Poggianti & van Gorkom 2001).

1.2 Star-formation in the radio continuum

One way of determining the star-formation rate of a galaxy is by looking at its spectral properties (see the previous section), together with its blue luminosity (since young stars are blue). However, this method may not be very accurate because of extinction of massive stars in giant molecular clouds in which they are born, which is true for both the spectral lines and the blue luminosity. Furthermore, stars with a variety of different ages and spectral types can contribute to the blue luminosity of a galaxy (Sage & Solomon 1989). This method of calculating the SFR and even the way of classifying different galactic spectral types according to their star-forming activity may therefore be questionable. A strong debate has been going on between supporters of this method (e.g. Balogh et al. 2000) and the people who think that dust may play too much of a role for the results to be reliable (e.g. Poggianti et al. 1999). An alternative could be given by the radio continuum emission.

When there is star-formation going on, massive stars are born that soon explode into supernovae. In the supernova remnants electrons are accelerated and radiate synchrotron emission, which can be seen in the radio. I refer to Condon (1992) for more information. This method of recognizing star-forming galaxies (from now on SFGs) has until recently not been used very often yet and no definitive answer has been given yet as to which method is the better one. In the field, several groups have compared radio continuum observations with existing galaxy survey observations (see e.g. Sadler et al. (2002), Condon et al (2002)), but each time either the optical spectra were used to classify star-forming galaxies (i.e. to distinguish SFGs from AGNs which also radiate in the radio) or no spectra were available. No comparison has therefore been made of the two methods.

Moving on from the field to clusters, Dwarakanath & Owen (1999) studied the radio properties of clusters Abell 2125 and 2645 ($z \sim 0.25$, richness class 4) at 20 cm wavelength (1.5 GHz). They found 27 radio sources in A2125 and 4 in A2645, of which about half show signs of star-formation, based only partly on spectral lines. The difference was blamed on the dynamical state of the clusters: A2125 is not relaxed yet and A2645 is. Optically, only six galaxies that are expected to be star-forming galaxies according to their radio flux have Hα and [OII] emission line strengths according to a star-forming

galaxy. For the other objects the line emission is much weaker. Some of these could in fact be AGNs, but several have colours consistent with spirals, so these are either spiral AGNs, or dust obscured star-forming galaxies (Owen et al, 2001). In any case, the fact that SFGs are found in the radio and not in the optical, means it is worthwhile to explore the radio method.
Recently, Miller & Owen (2002) published the results of a comparison of 20 nearby Abell clusters ($z \lesssim 0.25$), that have been observed in the radio at 1.4 GHz with the VLA. The classification of the SFGs however, was done through their optical spectra in this case too. This is despite the fact that they conclude themselves that the [OII] emission line (and any other line) may sometimes not be visible due to dust-extinction.
Finally, Morrison & Owen (2003) have worked on a sample of 30 rich Abell clusters out to a redshift of ~ 0.08, using radio continuum emission at 1.4 GHz. No spectra are available however, so no comparison could be made between optical and radio results.
Overall, both the Miller & Owen and the Morrison & Owen results suggest less star-formation activity at low redshift than MORPHS had found near z=0.5. This is in accordance with the Butcher-Oemler effect. Still, the question on how this suppression arises remains unanswered.

The main goal of this project is to study the star-formation properties of the cluster of galaxies Abell 2670 using radio 20 cm observations, compare the results with those of other clusters and to try to recognize the processes responsible for the results. These processes could then be responsible for the evolution on star-formation that galaxies undergo, and hence the Butcher-Oemler effect. Also, spectra and classifications following table 1 have already been made. A second goal therefore, is to compare the results obtained in the radio with the results obtained using optical spectra.
In section 2 some brief information is given about A2670. In section 3 the method of classifying SFGs in the radio continuum and determining their SFR and other properties will be explained. Section 4 states the results of both the radio and the optical method and in section 5 the results of the star-formation activity according to the radio method will be discussed. A comparison of the radio sample with the optical sample and a comparison of the results will be made in section 6. Finally the conclusions follow in section 7.

2 Abell 2670

The cluster of galaxies Abell 2670 is at a redshift of 0.0767 the nearest Abell cluster of richness class 3 (van Gorkom 1996). In the center of the cluster is a supergiant cD galaxy. The mean velocity of the cluster is 22843 ± 64 km/s, however the velocity of the central cD galaxy is 23282 ± 100 km/s. The cD galaxy may therefore not be at the dynamical center of the cluster, which could indicate mergings of subclusters. Sharples, Ellis & Gray (1988), who have performed a photometric and spectroscopic study of 303 galaxies centered on A2670, could find no statistical evidence of such subclustering. Bird (1994) however, used the observations of Sharples et al. and analyzed the velocity and position data of 230 galaxies of the list of 303 that she determined to be cluster members. From that she concluded that at least two and maybe three subclusters are currently merging along the line of sight.
So if A2670 is not completely virialized yet, then why would it be a good cluster to study evolution of galaxies? Apart from the fact that it is a relatively nearby yet rich cluster and therefore a good cluster to compare with MORPHS, A2670 is also an obvious choice because a lot of observations have been made of the cluster, at a lot of different wavelengths. As mentioned above, Sharples et al. took the optical spectra of 303 galaxies centered around A2670, 230 of which are cluster members whose spectra have been recently analyzed by B. Poggianti (see sections 3 and 6). Then, Hobbs & Willmore (1997) looked at the cluster in X-ray using the ROSAT satellite and Hansen et al. (1999) observed in the far-infrared, using the Infrared Space Observatory (ISO) satellite. Also, van Gorkom in collaboration with B.Poggianti, K. Dwarakanath, P. Guhathakurtha, A. Shambrook and R. Sharples obtained HI data down to a mass sensitivity of 10^8 $M_\odot$ (Poggianti & van Gorkom 2001) for the entire volume of the cluster. Finally, A. Shambrook (2001) made an extensive catalogue of the UBVRI colours of objects in an area of 1° x 1° centered on Abell 2670.
All these data make A2670 ideal for studying the star-formation properties of a cluster at low redshift. Also, the fact that the cluster is not relaxed should make it an all the more interesting case.

3 Method

3.1 Optical identification

The radio continuum observations at 20 cm of Abell 2670 that I have used came as a by-product of VLA HI data, obtained by the group of van Gorkom, Poggianti, Dwarakanath, Guhathakurtha, Shambrook and Sharples. With three pointings (North-East (NE), Center (C) and South-West (SW)) the entire volume of the cluster was mapped, covering the whole velocity space over an area of 5 Mpc^2, down to a limit of 10^8 $M_\odot$. The radio continuum images could be compared with optical images of the cluster, obtained with the CTIO 4-m telescope using the Big Throughput Camera (BTC) (Shambrook 2001). The three VLA pointings are shown in Figure 1. This image was made to correct the separate images for the primary beam effect, which causes the fluxes at the center of the images to be higher than at the edges. The AIPS task FLATN was used to combine the images. The correction for the primary beam effect also caused the noise to go up at the edges. Before the images could be combined though, the beam sizes had to be equalized, since FLATN will otherwise just take the resolution of one of the images, resulting in erroneous fluxes. To get the beam sizes equal, the NE and the SW image were convolved with the central image, which has the largest beam size, using AIPS task CONVL.
Figure 2 shows the combined image again, but now in blue roughly the area where the CTIO BTC images were taken of is plotted, and the red area is the area Shambrook observed with CTIO 0.9m/0.6m Curtis-Schmidt telescope in UBVRI colours. The latter observations resulted in a catalogue of $\sim$ 5300 galaxies in the direction of A2670. The + signs mark the positions of the galaxies in A2670 of which the spectra from Sharples et al. are known.
To determine which galaxies are reponsible for the radio continuum sources, contour-plots were made of the 20 cm emission over the optical BTC images. 75″ x 75″ finding charts have been made, an example of which can be seen in Figure 3. The beam of the radio images is roughly 25 x 30 arcseconds. The contour levels are multiples of the noise level (σ_{noise}), which is 62.0 μJy for the NE pointing, 32.5 μJy for the central pointing and 83.8 μJy for the SW pointing. The identification of the radio sources with galaxies from the catalogue of Shambrook is based on position coincidence. Galaxies that have been classified by Shambrook as "likely cluster member" (LM) or "possible cluster member" (PM) have been taken into account, where she used the redshift calculated using a photometric redshift analysis, which uses the measured UBVRI colours. This method is not highly accurate at low redshifts, so it is not unreasonable to think that a substantial number of "PMs" are in fact optically weak cluster members.
Note that not the whole VLA image is covered by the optical BTC images and neither by the CTIO Schmidt images. Outside this area I used images from the Digitized Sky Survey of the Space Telescope Science Institute to compare with the radio. Outside the Schmidt area however, I had no information on the galaxies present, except for a few galaxies observed by Sharples et al. At the edge of the combined VLA image the noise goes up and these regions were unsuitable for making any optical identifications. The total region taken into account is roughly given by an ellipse with a semi-major axis of

$\sim$3 Mpc and a semi-minor axis of $\sim$2 Mpc, centered near (RA, DEC) = (54 40, -10 20). Often the position coincidence is quite accurate and therefore the identification can be easily made (see e.g. Figure 3). The error in optical position of the galaxies (σ_{opt}) of the catalogue of Shambrook is 1 arcsecond. The accuracy of the radio position is $\sigma_{rad} \backsim$ 0.5*FWHM/(S/N), where (S/N) is the signal to noise ratio and the FWHM is $24.59''$. The total error σ_{tot} is given by $\sigma_{tot} = (\sigma_{rad}^2 + \sigma_{opt}^2)^{\frac{1}{2}}$. When identification is not immediately clear, I assume the sources are the same galaxy when both the radio and optical positions are within $2\sigma_{tot}$ of each other. Furthermore, I only looked at radio sources with a signal to noise ratio of 4 or higher (which is in the center equal to a luminosity of $1.5*10^{21}$ W/Hz), which automatically results in a smaller number of sources in NE and in SW than in the center, because of the different noise levels.
I have made a rough estimate of the possibility that a radio contour of $4\sigma_{noise}$ (and no higher) coincides with an optical galaxy by pure chance. This estimate was made for the center and for the North-East determining the average number of $4\sigma_{noise}$ radio contours (i.e. the contours with a flux no more and no less than between 4 and 5 σ_{noise}) in these regions per arcminute^2 and multiplying these numbers by the average area of a $4\sigma_{noise}$ contour. This was then multiplied by the average number of optical sources per arcminute^2. The result is the number of coincidental radio/optical matches per arcminute^2 for the center and for the North-East. Multiply this by the total area for both regions that optical identifications have been sought at and one gets the total number of accidental matches. The resulting estimate, is that $\backsim$ 0.1 radio source and optical source will coincidentally overlap in the center and $\backsim$ 0.04 in the North East. Note that the optical sources have been approximated by point sources, by taking the actual area of the sources on the images into account the estimate will be somewhat higher, but still the probability will be low especially since the radio/optical positions need to be within $2\sigma_{tot}$ of each other. The Southwestern image is not completely covered by the BTC images, so I could not make an accurate estimate there, but since the noise level in the SW is the highest of the three regions the chance will be even smaller. Therefore, the possibility that an identification is made by chance is effectively ruled out.
Sometimes two galaxies are close to each other or even interacting, making it harder to see which galaxy is the radio source. In Figure 4a, the center of the radio flux seems to be in between the two galaxies, which are a k/k+a/S0 galaxy (east) and a e(c)/Sc galaxy (spectral types determined by B. Poggianti, the morphologies by A. Shambrook). In this case, because the right one is optically classified as an SFG and the left one as a passive galaxy (and because on top of that spiral galaxies have a higher probability of being SFGs than earlier type galaxies, see next section), it is expected that the radiation arises from the left arm of the spiral galaxy, which is then where stars must be forming. Another example can be seen in Figure 4b. Here the Northern galaxy is classified as a k/S0 galaxy and the southern as k(e)/Sa. So both are optically observed as passive, but the radio flux is too low for the galaxies to be AGNs (see section 3.2), so they must both be forming stars. They are not resolved, but judging by the distortion to the right of the lower galaxy it is probable that they are interacting, which may be triggering the star-formation. This is a remarkable observation, since both galaxies were optically

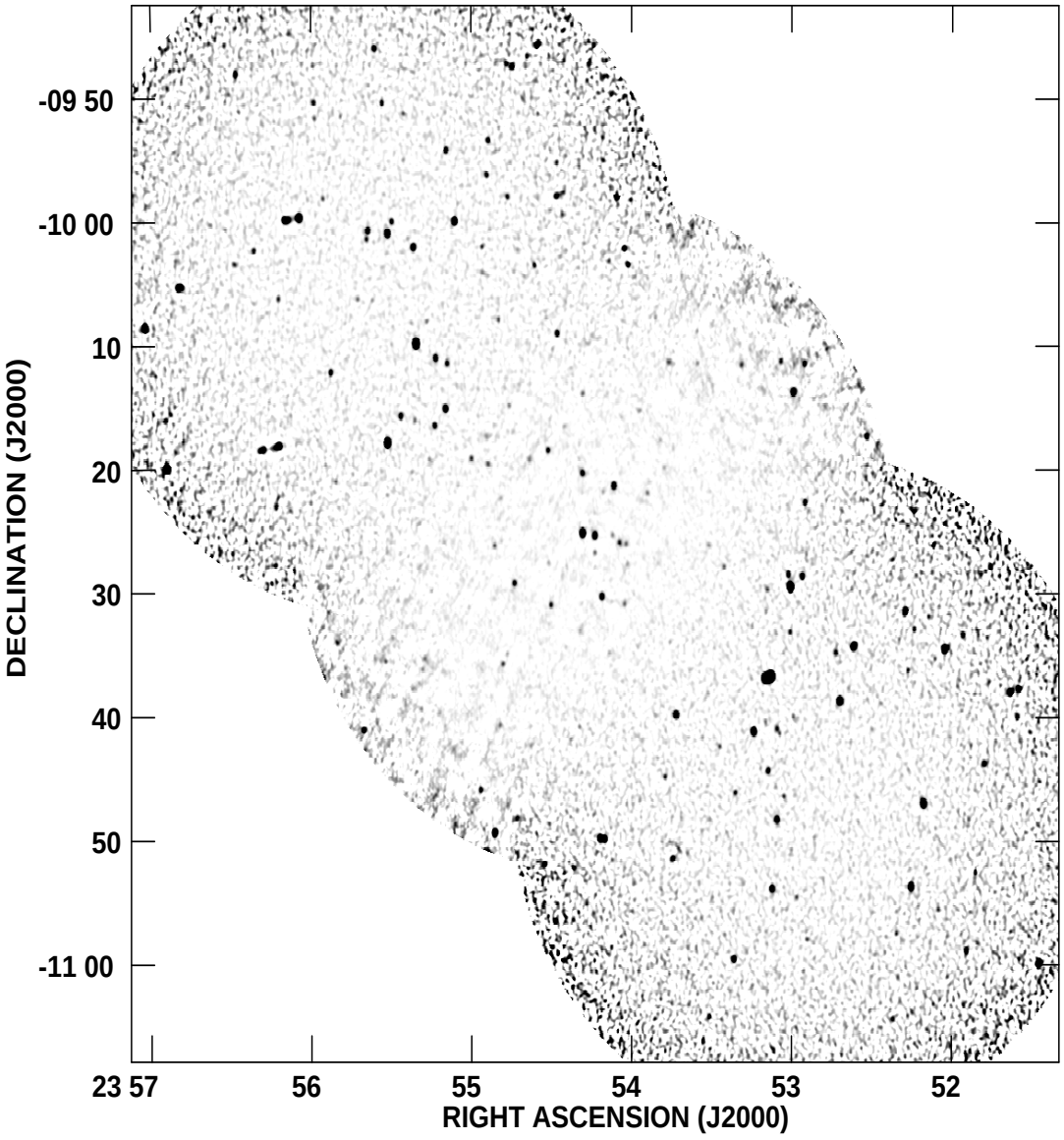

Figure 1: VLA pointings of Abell 2670, at 20 cm wavelength.

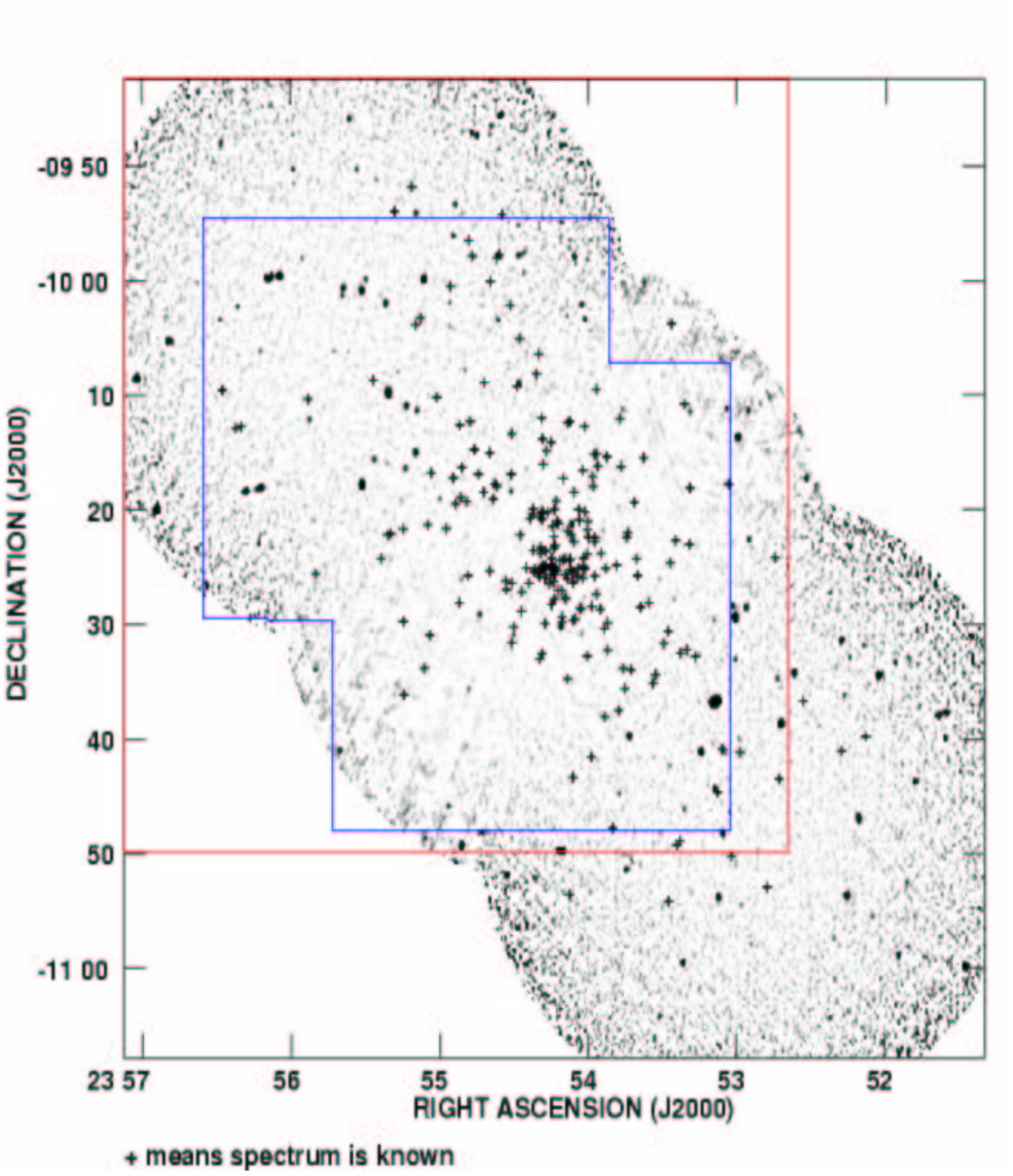

Figure 2: VLA pointings of Abell 2670 at 20 cm wavelength. Overplotted are in red the area of the CTIO Schmidt images and in blue the CTIO BTC images. The plus signs mark the positions of the galaxies in A2670 observed by Sharples et al.

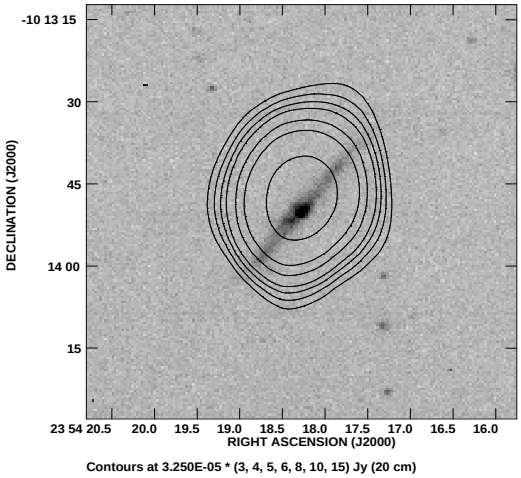

Figure 3: Radio 20 cm contours plotted over a BTC greyscale image. The galaxy is a Sb galaxy classified as e(c).

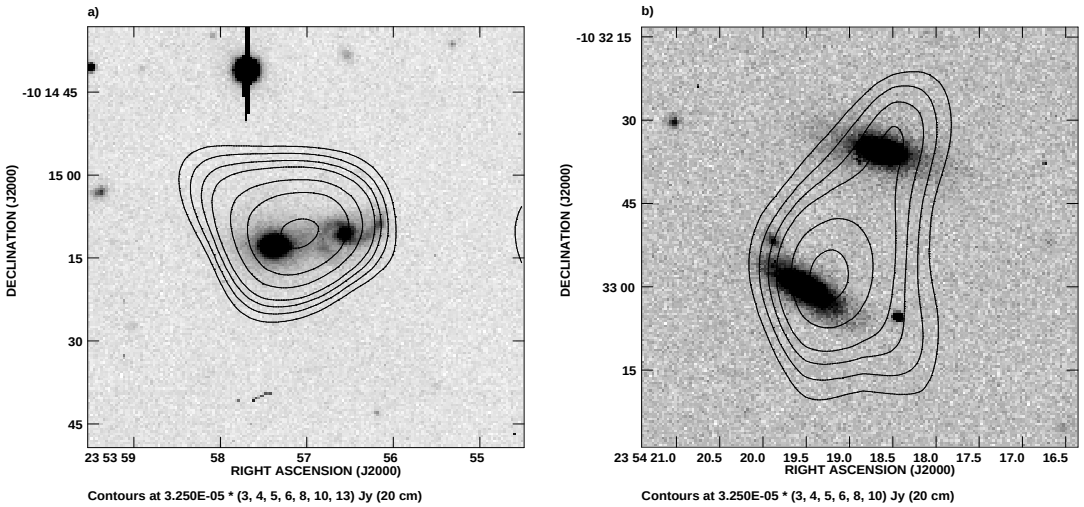

Figure 4: Interaction between galaxies. a) On the eastern side an Sa galaxy of spectral type k/k+a and on the western side an Sc galaxy of spectral type e(c). b) On the northern side an S0 galaxy of spectral type k and on the southern side an Sa galaxy of spectral type k(e).

classified as passive, although one is a k(e) galaxy, which means that hints of [OII] can be spotted. I will come back to this in section 6.

3.2 AGN versus star formation

Radio emission from star forming galaxies had to be distinguished from AGNs, which also emit in the radio. To distinguish between those two groups of galaxies it was assumed that the elliptical galaxies which are visible in the radio are AGNs, and that the spiral galaxies are star-forming galaxies (SFGs) (see e.g. Smail et al. 1999). The fact that this is not a waterproof method, is for instance confirmed in Figure 10 of Dressler et al. (1999), which shows that some (though very few) elliptical galaxies may still be forming stars. On the other hand, AGNs are usually ellipticals or S0's. The Hubble type of the galaxies of A2670 were taken from the catalogue of A. Shambrook. She determined the best spectral energy distribution (SED) type for $\backsim$ 5300 galaxies using a photometric redshift analysis of the observed UBVRI colours. An SED type can be used as an indicator of the morphological type, which is what I did.
To classify the galaxies as accurately as possible, the type of galaxies one has to look at in particular are the intermediate Hubble type galaxies, the S0 and also the Sa galaxies, because they are on the border of being either spiral or elliptical. I have used four criteria for a radio loud S0 or Sa galaxy to be classified as a SFG. First, if the optical classification by Poggianti is known and is determined to be an e(a), e(b), e(c) or e galaxy, then I took over this classification. Also, a low bulge-to-disk ratio and gravitational interaction between two galaxies (see Figure 4) were used as indications of star-formation. Finally, when a galaxy has a radio luminosity of $\log L_{20\mathrm{cm}} < 22.3$ it was considered a SFG, otherwise as an AGN. Below this luminosity the AGN contamination will be very low, SFGs with higher luminosity than this have been searched for too and found. Note that non of the above criteria is binding, usually the final classification was made after weighing the outcome of all four criteria. This obviously leaves room for bias, but on the other hand a careful one-by-one classification as was done here is the best way to get a complete sample of SFGs, without contamination of AGNs.

4 Results

I have identified 46 star-forming galaxies in Abell 2670. Their data are shown in Table 2, in order of increasing RA. Columns (1), (2), (4), (5) and (6) are taken from Shambrook, for details I refer to her thesis report. Column (11) is courtesy of van Gorkom. The following data are given in the columns:

(1) Right Ascension (J2000) in units of hours, minutes and seconds.
(2) Declination (J2000) in units of degrees, arcminutes and arcseconds.
(3) Luminosity at 20 cm with its error (in units of 10^{21} W/Hz). A Hubble constant of 75 km/s/Mpc and a redshift of 0.0767 are used throughout this report.
(4) Visual magnitude.
(5) Classification of "likely cluster member" (LM) or "possible cluster member" (PM).
(6) Spectral energy distribution type according to Shambrook, used as Hubble type in this report.
(7) Spectral type of the SFG, if known, as classified by B. Poggianti where she used the spectra of Sharples et al. (1988). A colon after a given type means that the classification is not certain. When two classifications are given divided by a dash, then the classification is uncertain, but the first one is the most probable.
(8) Projected distance to the central cD galaxy of A2670, given in Mpc. The central cD galaxy is located at RA = 23 54 13.66 and DEC = -10 25 10.25.
(9) Star formation rates and errors in Solar Mass per year, defined by SFR($M_\odot$/yr) = $5.9 \pm 1.8 * 10^{-22} L$ (Yun et al. 2001). (10) Subcluster membership according to Bird (1994), if known, based on the velocities of the individual galaxies determined by Sharples et al.
(11) HI mass, in $10^9 M_\odot$.
(12) Galaxy surface density Σ. The density for each SFG is the number of LM galaxies from Shambrook's catalogue within a radius of 0.5 Mpc of the SFG. A radius of 0.5 Mpc gives an area of $\sim$ 0.8 Mpc^2. When part of this area lies outside the area of the CTIO Schmidt images where Shambrook's catalogue is based on, then the density was adjusted for that by interpolation of the density at the edge of the image.

The only galaxy in Table 2 which is not in Shambrook's catalogue is at (RA, DEC) = (23 53 24.19, -10 49 17.24), which is outside the BTC images. Using a DSS image the identification could be made. Sharples also found the galaxy, so a spectral classification is available, and judged by its velocity (21947 km/s (Sharples et al.)) it can be classified as a likely cluster member.

My own results can be compared with the results of the spectral classification which was done by B. Poggianti. She used the $\sim$ 300 spectra Sharples et al. had taken of galaxies of A2670 and classified the galaxies following the scheme of Table 1, but using other star-formation indicators as well, like [OIII] and Balmer Hβ. Table 3 shows the data of all the galaxies from the list of Sharples, that have been optically classified as star-forming galaxies by Poggianti and that are also members of A2670 with known EW[OII] (of 2 galaxies that were classified as SFGs the EW[OII] could not be measured, they

are not in this table as their SFR could not be obtained) . They are again tabulated in order of increasing RA. Columns (1) and (2) are from Sharples et al., (3), (5) and (6) are from Shambrook and the data in columns (4), (7), and (8) were determined by Poggianti using Sharples' spectra. The columns list:

(1) Right Ascension (J2000) in units of hours, minutes and seconds.
(2) Declination (J2000) in units of degrees, arcminutes and arcseconds.
(3) Spectral energy distribution type ("Inc" stands for "Increasing starburst", consider these as spiral galaxies). In this report they are used as Hubble types.
(4) Spectral type.
(5) B magnitude.
(6) V magnitude.
(7) Equivalent width of the [OII] line.
(8) Equivalent width of the Hδ line.
(9) Star formation rate in Solar Mass per year, obtained using $L_{20\mathrm{cm}}$, with error.
(10) The projected distance to the central cD galaxy in Mpc.
(11) Optical star formation rate in Solar Mass per year, calculated by using the equivalent width of the [OII] emission line (see Barbaro & Poggianti 1997):

$$SFR(M_{\odot}/yr) = 6.3 * 10^{-41} L_{[\mathrm{OII}]} \tag{1}$$

with

$$L_{[\mathrm{OII}]} = (1.4 \pm 0.3) * 10^{29} \frac{L_B}{L_{B_{\odot}}} * \mathrm{EW[OII]} \tag{2}$$

Here, L_B is the blue luminosity and $L_{B_{\odot}}$ is the blue luminosity of the Sun.
(12) The ratio of the two SFRs, if applicable.
(13) Galaxy surface density within 0.5 Mpc of each optical SFG. As for the radio SFGs, the density was adjusted for when the area was partly outside the CTIO Schmidt range. Also, two SFGs were outside the CTIO Schmidt area altogether. In those cases the density of the SFG nearest to them was taken. They are indicated by a *.

RA(J2000)	DEC(J2000)	($L_{20cm} \pm \sigma$)[a]	V	PM/LM	HT	Spectral Type	d(Mpc)	SFR[b] $\pm \sigma$	Subcl.	HI[c]	Σ
23 53 05.64	-10 40 58.47	20.4 ± 1.0	17.15	LM	Sc	k(e):	2.071	12.0 ± 3.7	C	7.4	23
23 53 08.99	-10 29 42.47	11.3 ± 1.2	17.67	LM	S0		1.499	6.7 ± 2.2			28
23 53 19.99	-10 32 18.87	1.8 ± 1.0	17.47	LM	Sa	e(c)	1.357	1.1 ± 0.7	C		32
23 53 24.19	-10 49 17.24	6.3 ± 1.0	18.31	(LM)[d]		e(b)	2.418	3.7 ± 1.3	C		17
23 53 26.38	-10 15 51.05	3.7 ± 0.7	18.82	PM	Sa		1.343	2.2 ± 0.8		8.7	29
23 53 30.43	-10 21 38.94	2.2 ± 0.6	20.40	PM	Sc		1.015	1.3 ± 0.5			25
23 53 32.37	-10 38 29.55	3.4 ± 0.9	18.67	PM	Sc		1.503	2.0 ± 0.8			28
23 53 33.74	-10 41 33.29	4.8 ± 1.0	19.85	LM	Sb		1.711	2.8 ± 1.0			23
23 53 37.97	-10 36 09.95	4.0 ± 0.9	17.96	LM	Sb		1.263	2.4 ± 0.9			32
23 53 45.65	-10 33 55.28	3.9 ± 0.8	17.12	LM	Sa	e(c)	1.000	2.3 ± 0.8	A		34
23 53 45.88	-10 45 50.07	6.7 ± 1.2	18.52	LM	S0		1.944	4.0 ± 1.4			30
23 53 47.67	-10 19 45.41	4.5 ± 0.6	19.67	PM	Sc		0.755	2.6 ± 0.9			51
23 53 51.98	-10 32 19.00	3.1 ± 0.6	18.85	LM	S0	e	0.800	1.8 ± 0.6	A		40
23 53 56.58	-10 15 12.25	5.9 ± 0.7	17.55	LM	Sc	e(c)	0.967	3.5 ± 1.1	C		46
23 53 57.58	-10 34 18.10	3.2 ± 0.7	20.61	PM	Sc		0.890	1.9 ± 0.7			34
23 54 02.08	-10 26 00.65	8.2 ± 0.6	17.30	LM	S0a	e(c)	0.269	4.8 ± 1.5	C		90
23 54 02.73	-10 28 17.13	2.2 ± 0.6	18.32	PM	Sc		0.370	1.3 ± 0.9			74
23 54 02.92	-10 27 56.13	2.2 ± 0.6	18.15	LM	Sa		0.344	1.3 ± 0.9			77
23 54 04.57	-10 25 51.40	15.2 ± 0.6	17.46	LM	Sb	e(c)	0.211	9.0 ± 2.8	C		94
23 54 13.55	-10 27 50.08	2.0 ± 0.6	18.03	LM	Sc	e(c)	0.237	1.2 ± 0.5	B		81
23 54 13.57	-10 23 26.26	2.1 ± 0.6	17.13	LM	S0a	e(c)	0.155	1.2 ± 0.5	B		95
23 54 16.25	-10 20 18.16	2.0 ± 0.6	18.31	LM	Sa	e(c)/k+a(e)	0.438	1.2 ± 0.5	C		83
23 54 18.22	-10 13 51.01	7.7 ± 0.7	18.08	LM	Sb	e(c)	1.015	4.5 ± 1.4	A	6.5	38
23 54 18.33	-10 20 16.37	25.7 ± 0.6	17.50	LM	S0	e(b)	0.449	15.1 ± 4.6	B		79
23 54 18.60	-10 32 37.22	4.0 ± 0.6	16.72	LM	S0	k	0.673	2.4 ± 0.8	C		27
23 54 19.48	-10 33 01.44	6.7 ± 0.6	17.05	LM	Sa	k(e)	0.712	3.9 ± 1.2	B	1.6	23
23 54 24.14	-10 18 02.47	1.7 ± 0.7	20.07	PM	Sc		0.678	1.0 ± 0.5			49
23 54 30.59	-10 32 26.58	1.8 ± 0.6	19.82	PM	Sa		0.750	1.1 ± 0.5			23
23 54 32.20	-10 07 06.95	3.0 ± 1.0	21.19	PM	Sc		1.663	1.8 ± 0.8			24
23 54 33.27	-10 32 08.36	2.9 ± 0.6	20.59	PM	Sc		0.760	1.8 ± 0.6			22
23 54 35.36	-09 56 49.19	3.1 ± 1.5	17.98	LM	Sc		2.574	1.9 ± 1.0			24
23 54 35.64	-10 27 17.47	1.6 ± 0.6	19.45	PM	Sc		0.526	0.9 ± 0.4			47
23 54 38.13	-10 19 09.19	9.4 ± 0.7	17.29	LM	Sa	e(c)	0.766	5.5 ± 1.7	C	4.4	34
23 54 44.12	-10 16 57.26	4.4 ± 0.8	17.81	LM	Sc	e(c)	1.000	2.6 ± 0.9	A	8.9	30
23 54 45.72	-09 55 09.08	4.1 ± 0.9	18.17	LM	Sc		2.771	2.4 ± 0.9			26
23 54 45.79	-10 14 47.07	6.1 ± 0.8	17.50	LM	Sd	e	1.171	3.6 ± 1.2	A	0.3	29
23 54 50.93	-10 16 22.92	2.9 ± 0.7	18.20	LM	Sc	e(c)	1.143	1.7 ± 0.7	A	1.5	31
23 54 53.56	-10 19 32.67	9.5 ± 0.7	18.24	LM	Sc	e(a)/e(c)	1.022	5.6 ± 1.8	C	1.2	28
23 54 54.11	-10 17 18.01	9.2 ± 0.7	16.70	LM	Sb	e(c)/e(a)	1.143	5.4 ± 1.7	A	7.8	31
23 54 55.86	-10 01 59.10	10.7 ± 0.9	17.80	LM	Sc		2.272	6.3 ± 2.0			29
23 55 04.87	-10 21 21.61	3.1 ± 0.7	17.49	LM	Sb	e	1.192	1.8 ± 0.7	A		22
23 55 14.37	-10 33 25.14	2.1 ± 0.8	18.28	PM	Sa		1.542	1.3 ± 0.6			15
23 55 14.68	-10 29 48.40	3.5 ± 0.8	17.73	LM	Sa	k:k+a	1.422	2.0 ± 0.8	B		11
23 55 29.58	-10 09 47.05	3.3 ± 0.8	18.18	LM	Sa		2.180	1.9 ± 0.7			25
23 55 37.10	-10 06 16.13	4.9 ± 0.8	17.66	LM	Sd		2.512	2.9 ± 1.0			24
23 56 19.85	-10 12 47.21	4.5 ± 1.1	17.41	LM	Sb	e(c)/e(a)	3.025	2.6 ± 1.0	A		21

Table 2. Star forming galaxies in Abell 2670, as determined by their radio flux.
[a]) $*10^{21}$ W/Hz. [b]) units of $M_\odot$/yr. [c]) $*10^9 M_\odot$. [d]) This galaxy is positioned outside the BTC images

RA(J2000)	DEC(J2000)	HT	Spectral Type	B	V	EW[OII]	EW(Hδ)	$SFR^a_{rad} \pm \sigma$	d(Mpc)	$SFR^a_{opt} \pm \sigma$	$\frac{SFR_{rad}}{SFR_{opt}}$	Σ
23 52 33.05	-10 36 41.3	u	e(c)	19.22	18.97	-31.5	3.2		2.468	0.83 ± 0.21		20*
23 52 44.54	-10 24 11.0	S0a	e	19.80	18.71	-25.0			1.991	0.39 ± 0.10		20
23 53 20.05	-10 32 16.6	Sa	e(c)	18.51	17.47	-12.1	3.3	1.1 ± 0.7	1.356	0.62 ± 0.14	1.7	32
23 53 20.99	-10 10 47.4	Inc	e(c)	19.68	19.02	-34.4			1.741	0.59 ± 0.13		22
23 53 24.14	-10 49 17.2	u	e(b)	18.52	18.31	-59.7	3.0	3.7 ± 1.3	2.418	3.00 ± 0.77	1.2	17
23 53 26.26	-10 03 49.4	Sc	e	20.16	19.61	-16.9			2.177	0.19 ± 0.06		22
23 53 44.01	-10 22 01.3	Inc	e(b)	19.31	18.91	-104.0	9.1		0.718	2.54 ± 0.56		42
23 53 45.70	-10 33 53.7	Sa	e(c)	18.13	17.12	-14.5		2.3 ± 0.8	0.999	1.04 ± 0.23	2.2	35
23 53 51.94	-10 32 17.6	S0	e	20.20	18.85	-7.4		1.8 ± 0.6	0.799	0.08 ± 0.02	23.0	40
23 53 52.40	-10 15 26.0	Sc	e(c)	19.85	19.15	-35.4			0.991	0.53 ± 0.12		43
23 53 54.56	-10 23 50.0	S0a	e(c)	19.50	18.35	-8.4	2.8		0.442	0.17 ± 0.04		78
23 53 56.48	-10 15 10.8	Sc	e(c)	18.25	17.55	-6.8	3.6	3.5 ± 1.1	0.970	0.44 ± 0.11	7.9	46
23 53 56.71	-10 09 30.6	Sd	e(a)/e(c)	19.66	19.11	-27.1	3.2		1.446	0.48 ± 0.10		26
23 53 57.20	-10 25 50.2	Sc	e(b)	19.83	19.15	-52.9			0.372	0.80 ± 0.20		87
23 53 58.16	-10 17 07.5	Sc	e(c)	19.27	18.32	-7.8	2.5		0.797	0.20 ± 0.04		54
23 53 58.41	-10 28 27.5	Sc	e(a)	19.91	19.08	-19.9	4.9		0.448	0.28 ± 0.06		67
23 54 00.33	-10 23 52.8	Sb	e(a)/e(c)	19.82	19.00	-17.3			0.322	0.26 ± 0.06		98
23 54 01.76	-10 24 13.7	Sa	e(c)/e(a)/k+a	19.88	18.70	-3.7	3.8		0.280	0.05 ± 0.02		97
23 54 02.00	-10 25 58.8	S0a	e(c)	18.31	17.30	-11.5	2.8	4.8 ± 1.5	0.269	0.70 ± 0.15	6.9	90
23 54 04.39	-10 25 50.2	Sb	e(c)	18.26	17.46	-10.0		9.0 ± 2.8	0.213	0.64 ± 0.15	14.0	94
23 54 05.84	-10 26 24.7	Sc	e(a)/k+a(e)/e(c)	20.06	19.30	-4.6	3.5		0.208	0.06 ± 0.01		93
23 54 06.79	-10 22 15.3	Sb	e(c)	19.49	18.52	-10.4	0.7		0.301	0.22 ± 0.05		92
23 54 07.53	-10 53 38.1	u	e	19.00	18.85	-18.5			2.542	0.60 ± 0.15		17*
23 54 08.96	-10 27 49.0	Sa	e	19.79	18.75	-12.9			0.259	0.20 ± 0.05		84
23 54 11.84	-10 21 15.5	Inc	e(b)	19.97	19.53	-25.4	2.9		0.352	0.34 ± 0.07		91
23 54 13.51	-10 27 48.6	Sc	e(c)	18.84	18.03	-10.5		1.2 ± 0.5	0.235	0.39 ± 0.09	3.0	81
23 54 13.75	-10 23 24.4	S0a	e(c):	18.16	17.13	-6.8		1.2 ± 0.5	0.157	0.48 ± 0.11	2.5	95
23 54 16.38	-10 20 16.4	Sa	e(c)/k+a(e)	19.22	18.31	-4.7	3.3	1.2 ± 0.5	0.440	0.12 ± 0.03	9.6	83
23 54 18.30	-10 13 50.2	Sb	e(c)	18.91	18.08	-18.9		4.5 ± 1.4	1.016	0.66 ± 0.15	6.8	38
23 54 18.30	-10 20 14.3	S0	e(b)	18.69	17.50	-50.7		15.1 ± 4.6	0.452	2.19 ± 0.48	6.9	79
23 54 22.14	-10 19 56.6	Sc	e(c)	20.28	19.48	-7.2			0.502	0.07 ± 0.02		67
23 54 22.14	-10 20 22.5	Sc	e(a)	20.24	19.36	-14.4	6.8		0.468	0.15 ± 0.05		73
23 54 30.06	-10 30 15.5	Sd	e(c)	19.18	18.55	-16.2			0.581	0.44 ± 0.10		44
23 54 35.79	-09 57 46.4	Sd	e(b)	19.19	18.53	-54.1			2.493	1.47 ± 0.32		26
23 54 36.76	-10 17 58.5	Sc	e(c)	18.89	18.11	-12.8			0.824	0.46 ± 0.10		31
23 54 38.20	-10 19 08.0	Sa	e(c)	18.24	17.29	-7.5	2.2	5.5 ± 1.7	0.767	0.49 ± 0.11	11.3	34
23 54 39.39	-10 00 05.7	Sd	e(c)	19.04	18.37	-13.0			2.309	0.40 ± 0.09		29
23 54 44.19	-10 16 56.6	Sc	e(c)	18.55	17.81	-9.1		2.6 ± 0.9	1.001	0.45 ± 0.10	5.8	30
23 54 50.91	-10 16 22.0	Sc	e(c)	19.00	18.20	-35.6		1.7 ± 0.7	1.144	1.16 ± 0.26	1.5	31
23 54 53.55	-10 19 32.1	Sc	e(a)/e(c)	18.86	18.24	-24.8	4.5	5.6 ± 1.8	1.023	0.91 ± 0.20	6.1	28
23 54 54.27	-10 17 17.1	Sb	e(c)/e(a)	17.59	16.70	-6.2	5.2	5.4 ± 1.7	1.145	0.74 ± 0.17	7.3	31
23 55 04.82	-10 21 21.1	Sb	e	18.40	17.49	-3.3		1.8 ± 0.7	1.193	0.19 ± 0.04	9.7	22
23 55 06.03	-10 33 51.7	Sd	e(c)	18.65	18.10	-20.9			1.402	0.93 ± 0.21		16
23 55 09.61	-10 03 53.5	Sd	e(c)	18.61	18.02	-26.0			2.270	1.21 ± 0.27		35
23 55 14.18	-10 36 11.4	Inc	e(c)	19.69	19.06	-17.5			1.670	0.30 ± 0.07		17
23 55 18.00	-09 54 00.2	Sd	e(b)	19.43	18.79	-63.3	8.4		3.127	1.38 ± 0.33		15

Table 3. Star-forming galaxies in Abell 2670 as identified by their spectra.

[a]) units of $M_\odot$/yr.

*) Positioned outside CTIO Schmidt. The density of the nearest SFG is taken.

5 Discussion of the radio results

5.1 Rates, positions and densities

The positions of the star-forming galaxies are plotted on the radio image of the A2670 in Figure 5. The Star-formation rates of the 46 SFGs found in the radio are plotted against their projected distance from the central cD galaxy in Figure 6, with a histogram of this plot given in Figure 7. The morphological and spectral types of the galaxies are indicated in Figure 6, if they are known.
The most noticeable feature in Figure 6 is the concentration of SFGs around ~ 0.9 Mpc, all with a SFR below ~ 6 $M_\odot$ yr^{-1}. The histogram makes this all the more clear. It seems like the number of SFGs remains constant and low until ~ 1.7 Mpc from the center, peaks around 0.9 Mpc and then drops. Still, near the center quite a few SFGs remain present. The star-forming galaxy found nearest to the center is at a distance of 0.15 Mpc from the cD galaxy. The magnitude of the SFRs in Figure 6 differs quite heavily sometimes from galaxy to galaxy, even taking the errors into account. At a projected distance higher than ~ 1.5 Mpc few SFGs are found. The galaxy with clearly the highest SFR in that region of the plot is a supposedly passive galaxy, with only hints of [OII] emission (k(e):). Its contourplot can be seen in Figure 8. To the South-West of the galaxy there seems to be another object, which is only visible in the radio. This could be a distant quasar positioned behind the galaxy, that may enlarge the 20 cm flux measured from the galaxy. If that is the case, then the star-formation rate would be lower than indicated in Figure 6, and the galaxy would have a SFR in the same range as the rest of the SFGs.
Another galaxy with very high SFR is the e(b) galaxy at ~ 0.4 Mpc, i.e. within the radius of the peak at 0.9 Mpc. A contourplot is shown in Figure 9. The galaxy inside the radio contours on the right in figure 9 is also a SFG, though not such a radio loud one.
However, the fact that the SFR of a certain galaxy is higher than the SFR of another one, could also be the result of the former galaxy just being more massive. In order to get a good comparison, the SFRs versus distance are given again in Figure 10, but now normalized by their respective luminosities, in terms of solar luminosity ($L_\odot = 3.86 * 10^{33}$erg/s). The luminosities are based on the visual magnitudes, given in Table 2. The SFR of the e(b) galaxy at 0.4 Mpc has now considerably gone down and so has the k(e): galaxy. The SFRs of the galaxies near the center are also a lot less significant. Around a projected distance of 0.8 Mpc four PM galaxies stand out above the other SFGs. This makes sense, since these galaxies have high magnitudes their redshift could not be determined very accurately and hence they were classified as PMs. One could also argue that since their normalized SFRs are high compared to the average normalized SFR, this means that these galaxies are in fact not forming stars but are AGNs. However, they fit all the criteria to be SFGs and their low radio luminosities make it very unlikely that these galaxies are AGNs. Also, as mentioned before, the possibility that these are chance occurrences is very low. The most extreme case of these is the spiral PM galaxy near 1.7 Mpc of the center. Its contourplot is shown in Figure 11. Due to a large error

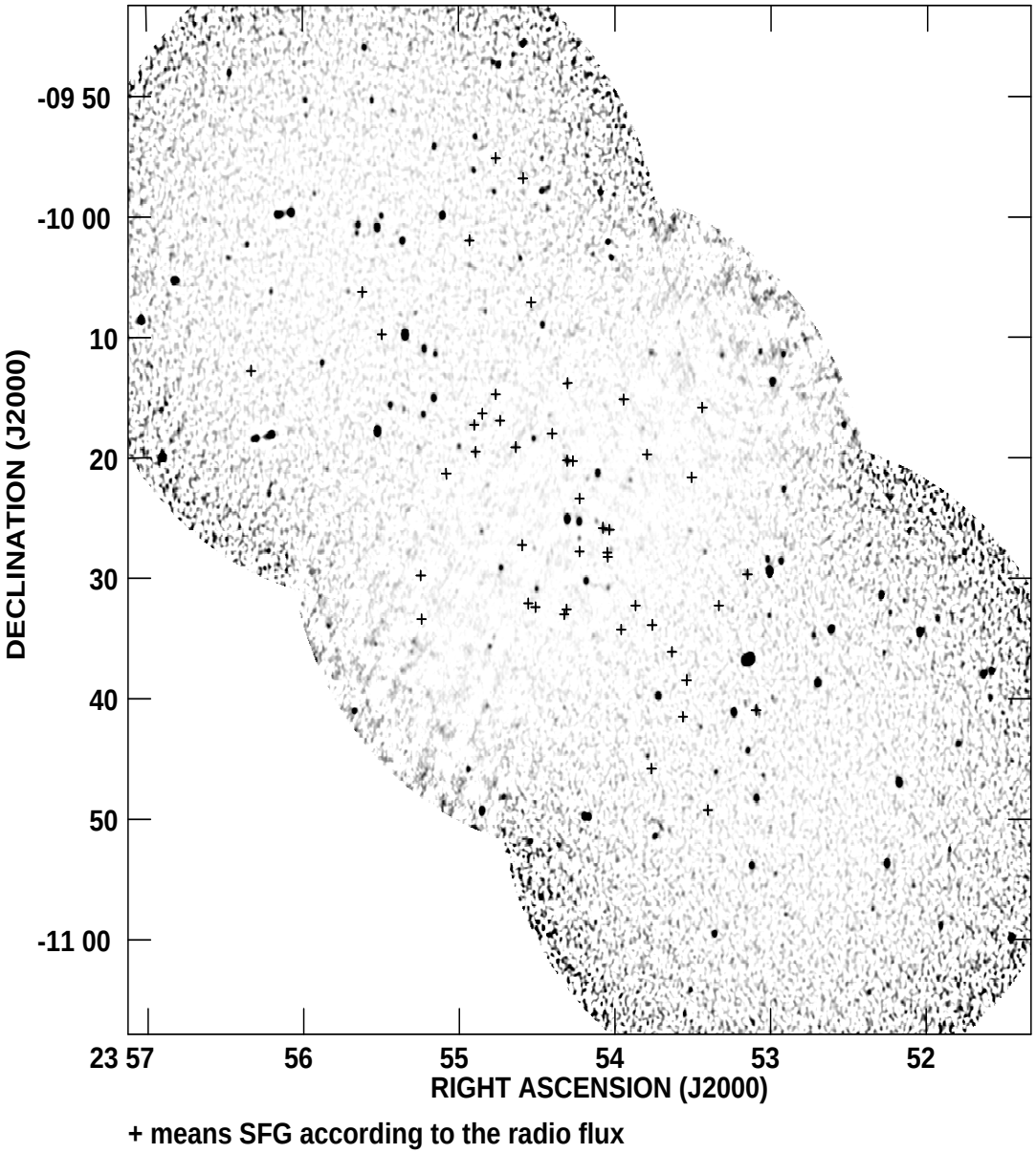

Figure 5: Positions of the SFGs plotted on the grey-scale image of the 20 cm radio continuum plot of A2670.

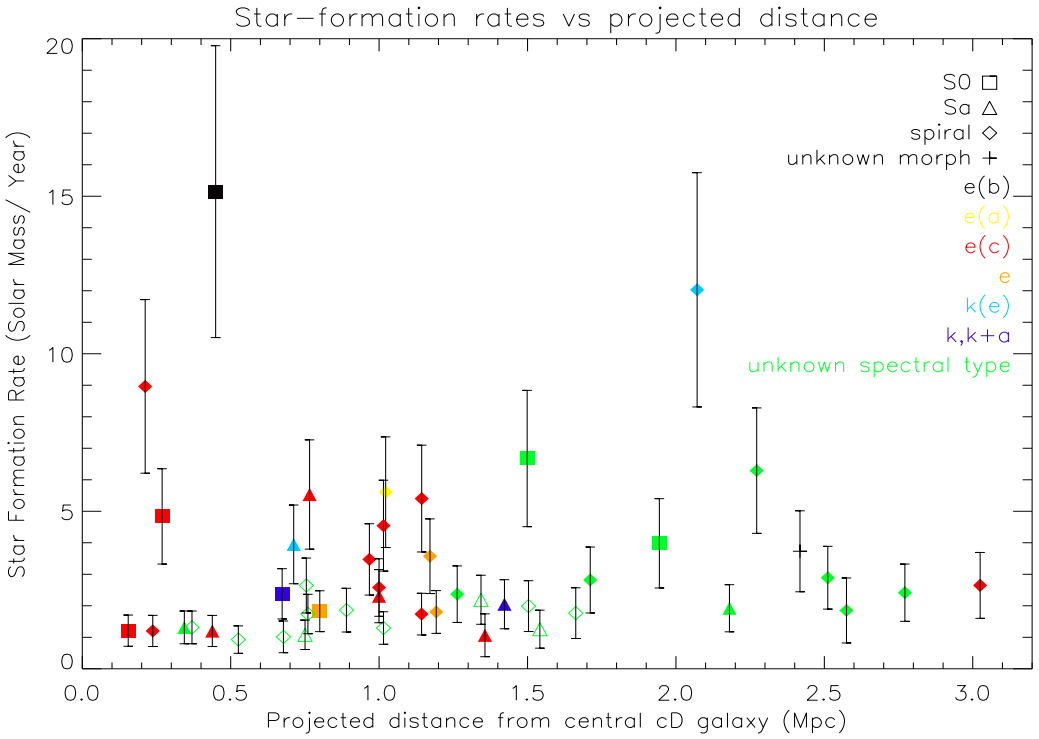

Figure 6: Star-formation rates plotted against projected distance from the cD galaxy. Spectral and morphological types are indicated. Closed symbols are LMs and open symbols are PMs.

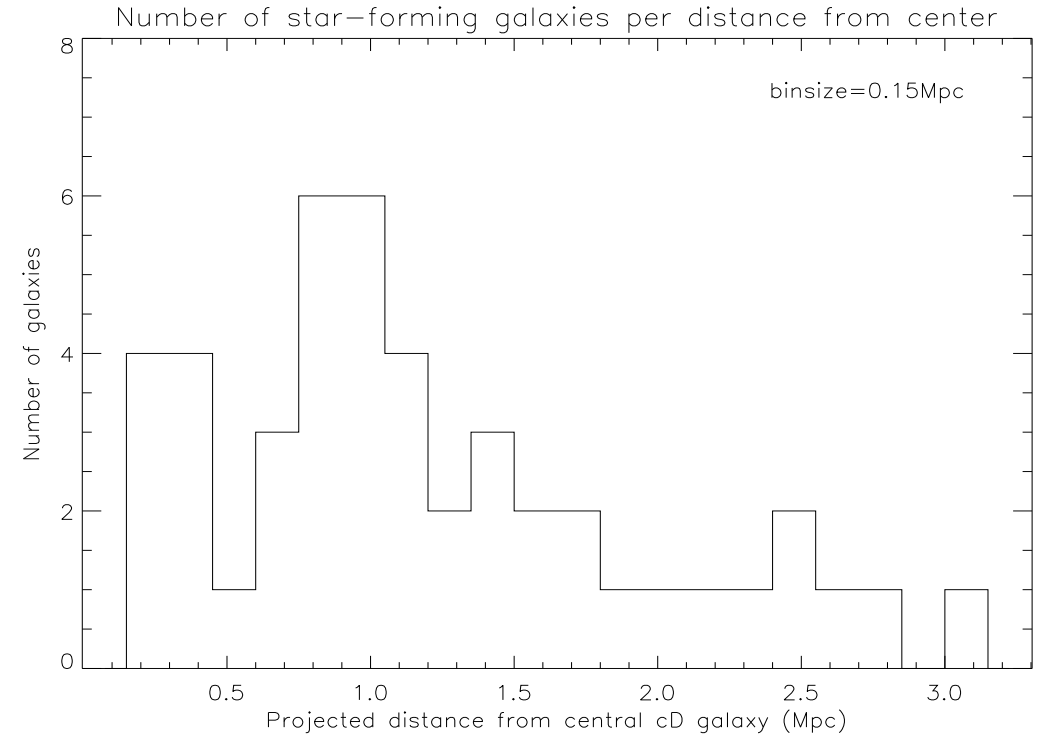

Figure 7: Histogram of the number of SFGs per 0.15 Mpc distance from the central cD galaxy.

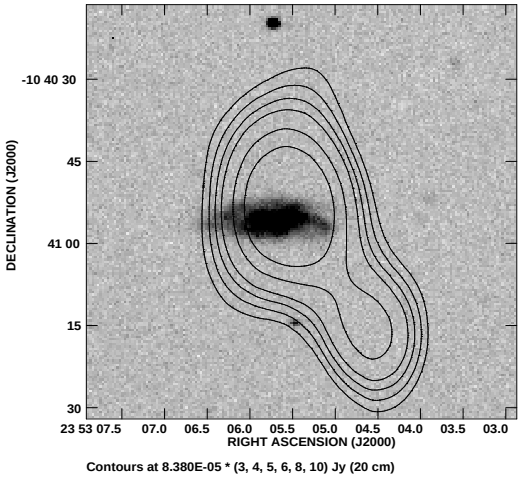

Figure 8: Radio 20 cm contours plotted over a BTC greyscale image. The galaxy is a Sc galaxy classified as k(e):. The object to the south-west of the galaxy could be a distant quasar

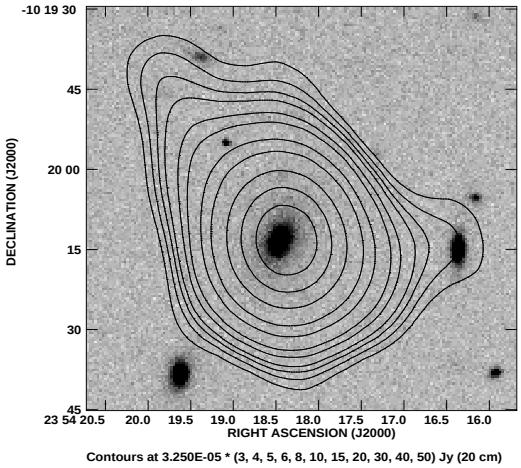

Figure 9: Radio 20 cm contours plotted over a BTC greyscale image. The galaxy is a S0 galaxy classified as e(b). The galaxy on the right inside the radio contours is also an SFG, this galaxy has a Hubble type Sa and is spectrally classified as e(c)/k+a(e).

in the visual magnitude, the error of its normalized SFR is very high, which makes it very well possible that the actual value should be much less, putting it in line with the rest of the galaxies. Figure 10 shows that not only the number of SFGs rises near 1 Mpc from the center while keeping low and constant farther out, but the same goes for the

SFR. After the peak around 0.9 Mpc, the normalized SFRs near the center are low.

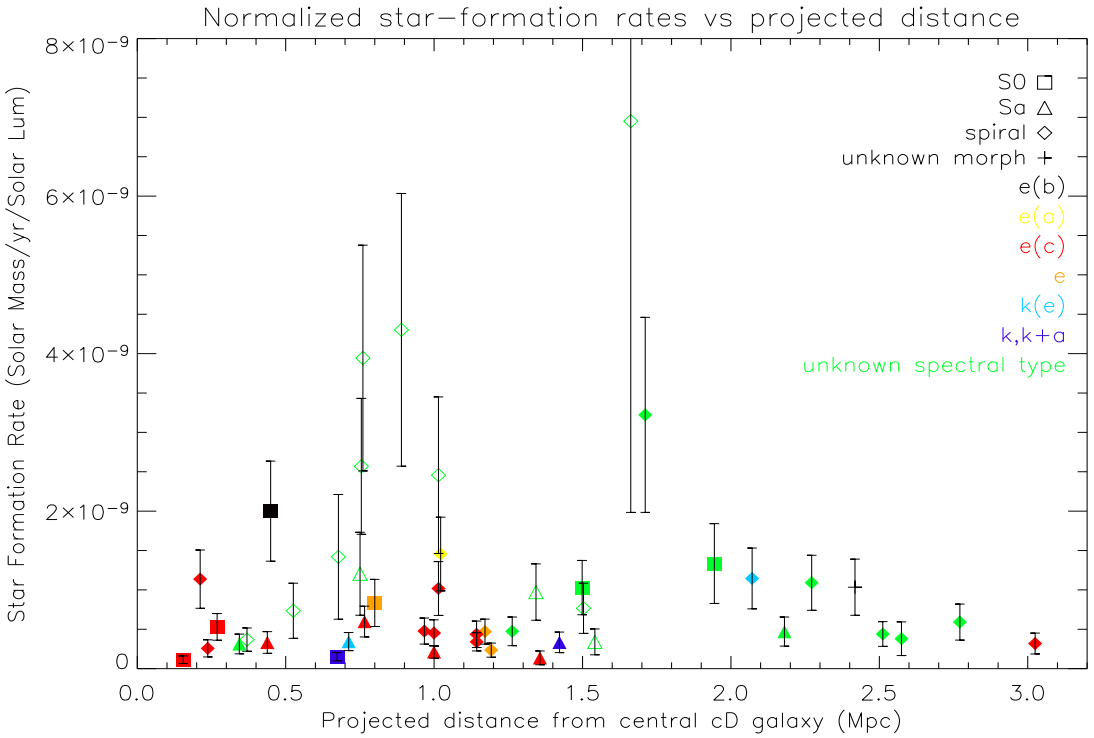

Figure 10: Star-formation rates divided by their respective luminosities in terms of solar luminosities, plotted against projected distance from the cD galaxy. $L_\odot = 3.86 * 10^{33}$erg/s. Spectral and morphological types are indicated. Closed symbols are LMs and open symbols are PMs.

Plotting the SFR versus the distance to the cluster center suggests the assumption that Abell 2670 is a virialized cluster with the cD galaxy at its center. However, according to Bird (1994) A2670 is actually a merger (along the line of sight) of three subclusters, which is still going on. This idea was confirmed by other authors, like Hobbs & Willmore (1997). On top of that, Sharples et al. already realized that the cD galaxy is not at the dynamical center. In other words, A2670 is probably NOT virialized yet, and therefore it is more beneficial to look at the SFRs plotted against galaxy surface density Σ, instead of projected distance. The results are plotted in Figure 12, for the exact numbers see table 2. The normalized SFRs versus galaxy density are given in Figure 14.
Roughly two groups can be distinguished in Figures 12 and 14. A very large group with $10 < \Sigma < 55$ and a small scattered group with $70 < \Sigma < 95$. The former group shows a clear pattern. It has a clear and narrow peak at a density of ~ 25 galaxies (see the histogram in Figure 13) and getting to higher density not only the number of galaxies drops but also the star-formation rates of those SFGs drop. It seems reasonable to say that there must be a mechanism at work that enhances star formation when the density gets to ~ 20 galaxies per 0.8 Mpc^2 and the same or another mechanism must also be

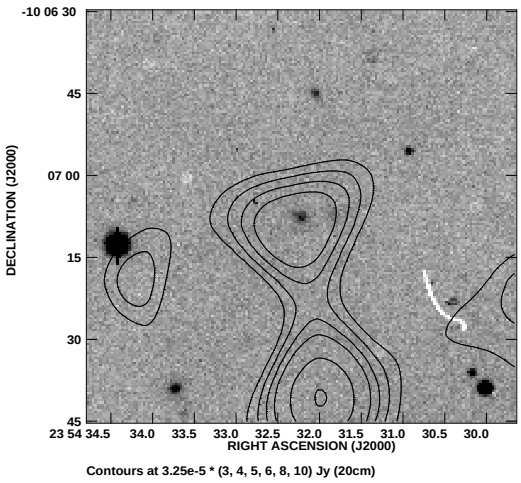

Figure 11: Radio 20 cm contours plotted over a BTC greyscale image. The galaxy is a Sc galaxy classified, not found by Sharples et al.

responsible for a drop in steep drop in star-formation rates after a density of $\sim$ 35 galaxies per 0.8 Mpc^2. The small group at high density consists of galaxies which are all within $\sim$ 0.5 Mpc of the cD galaxy. Also, all SFGs within that radius of 0.5 Mpc are to be found in the high density group, which means that both groups consist of the same population. Here, another mechanism may be at work.

To get a closer look of this area a contourplot of the area around the cD galaxy is shown in Figure 15. The area shown is 0.6 Mpc x 0.6 Mpc, centered at the cD galaxy. For the six SFGs in that area the spectral type, morphological type and subcluster membership are given. I will come back to this subcluster membership in the next section. Note that unfortunately the BTC images are not scaled correctly, which causes the greyscale objects to be apart from the position they should really be at compared with the radio contours. Especially the Sa and Sc galaxies are suffering from this misalignment, their positions should be slightly more to the North-East, in line with the radio contours.

As mentioned before, Hobbs & Willmore used the ROSAT satellite to observe A2670 in the X-ray. The resulting image can be seen in Figure 15, with overplotted HI contours. The X-ray region is fairly circular with a radius of $\sim$ 0.5 Mpc. This means that all the SFGs that are in the high-density group (and that are found at lower distance from the center than the peak at 0.9 Mpc), are in fact positioned in the X-ray region. The only starburst (e(b)) galaxy of the sample is found exactly at the edge of the X-ray.

Looking for answers on how to explain these results, it might be useful to compare them with the results from similar nearby galaxies, that have also been observed in the radio continuum.

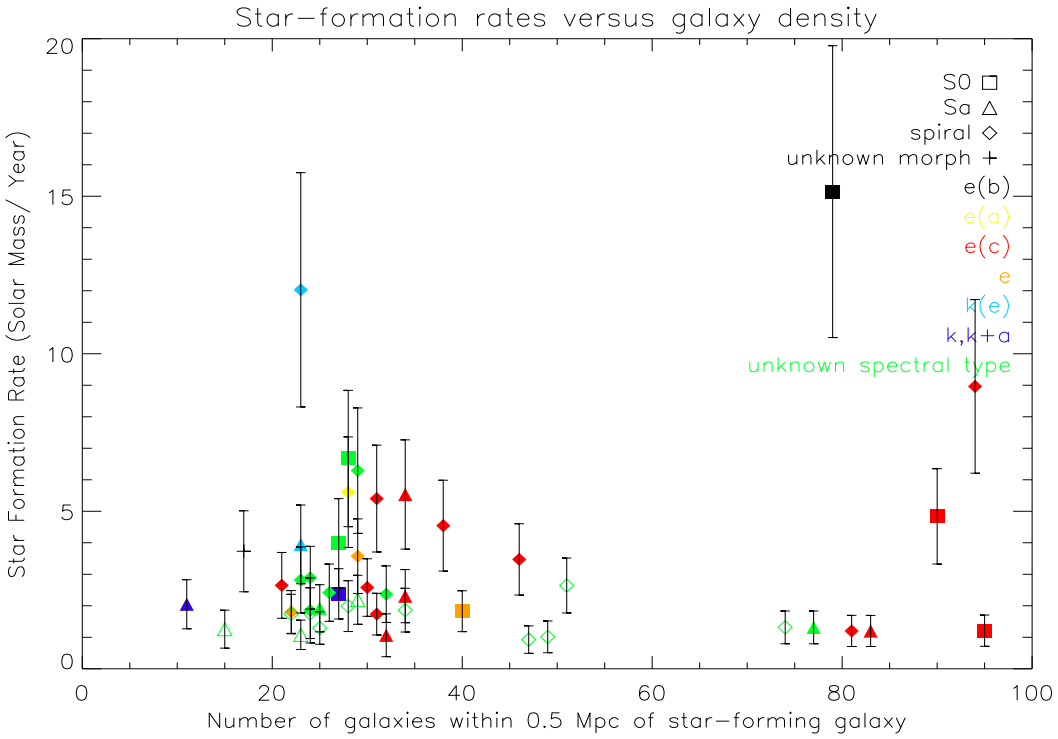

Figure 12: Star-formation rates plotted against the number of galaxies in a radius of 0.5 Mpc ($\sim$ an area of 0.8 Mpc^2). Spectral and morphological types are indicated. Closed symbols are LMs and open symbols are PMs.

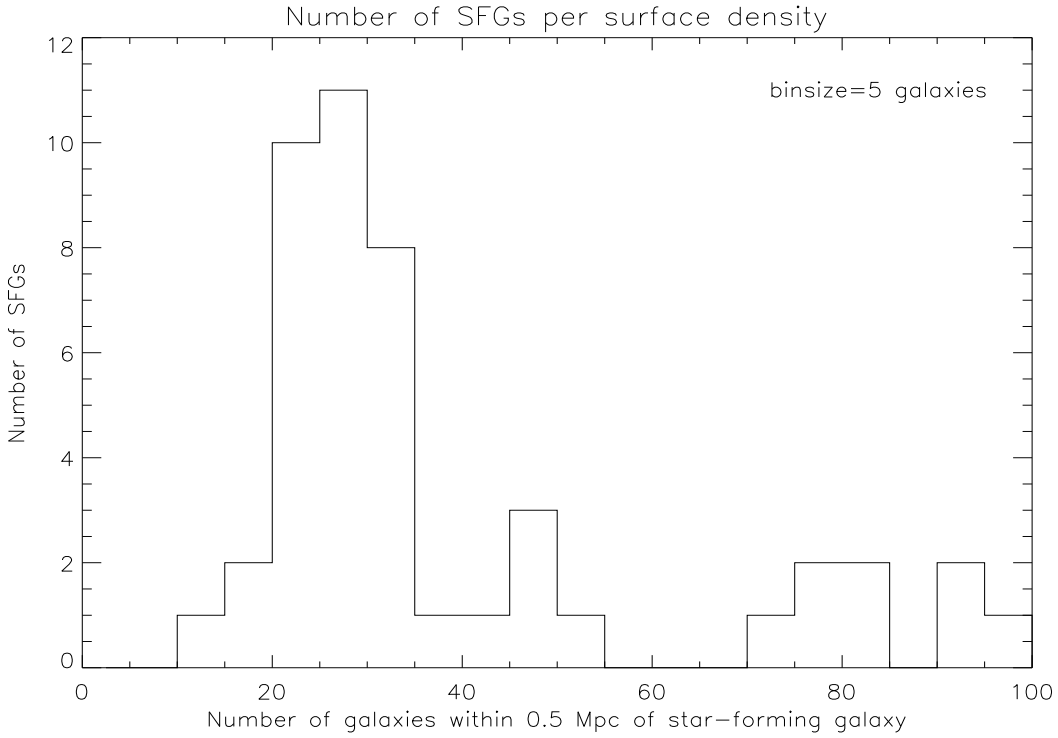

Figure 13: Histogram of the number of SFGs per galaxy surface density.

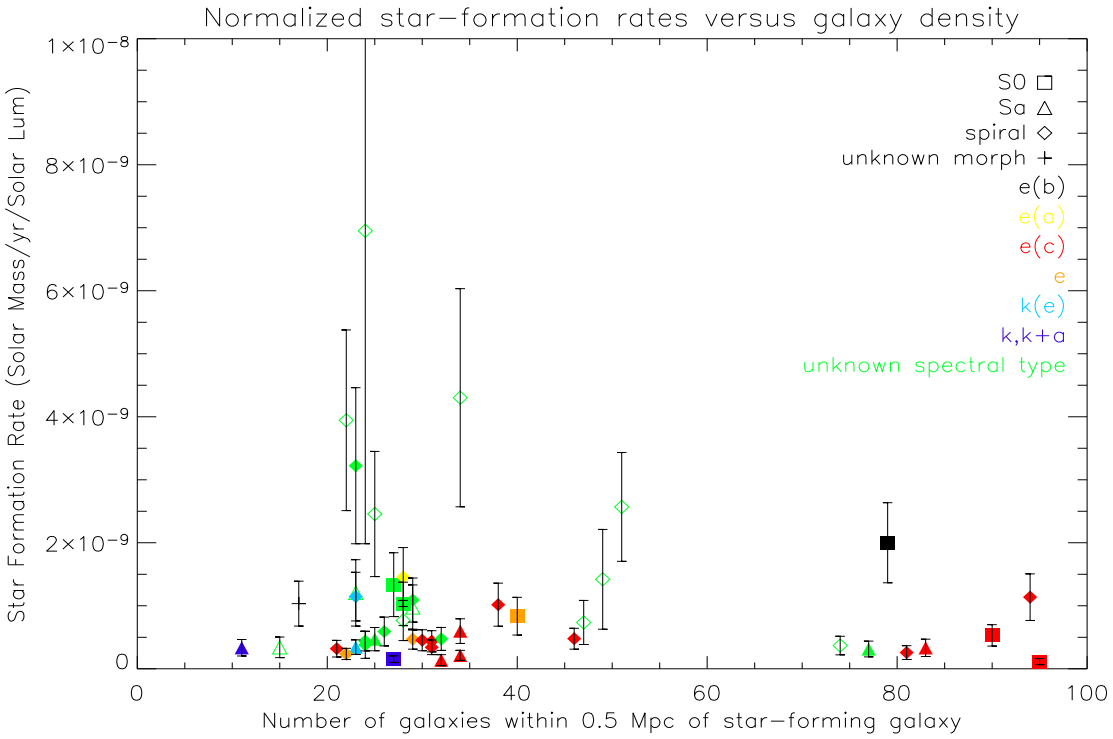

Figure 14: Normalized star-formation rates plotted against the number of galaxies in a radius of 0.5 Mpc (∼ an area of 0.8 Mpc^2). Spectral and morphological types are indicated. Closed symbols are LMs and open symbols are PMs.

5.2 Comparison with other clusters: mergers

Is A2670 any special compared to other clusters of galaxies? Two clusters that have previously been observed in the radio continuum are Abell 2125 and Abell 2645, both rich clusters at a redshift of ∼ 0.25 (Dwarakanath & Owen, 1999). Using the VLA they reached a luminosity limit for both clusters of $1.4*10^{22}$ W Hz^{-1}. Butcher & Oemler (1984) had already found that the blue galaxy fraction of A2125 (0.19) is considerably higher than that of A2654 (0.03), possibly indicating more star-formation in the former cluster. Indeed, they found 27 cluster members is the radio for A2125, of which 10 were identified as SFGs according to their emission lines, blue color and D_{4000} break, where in A2645 only 4 radio sources were found, none of which are galaxies forming stars. The difference in star-formation activity despite the similarities in redshift and richness and equal luminosity limits, was explained by the difference in the stage of evolution the clusters are in. A2645 seems to be a completely virialized. A2125 however, is still in the process of merging of different subclusters, which means that most cluster members still retain their gas content, opening the way to star-formation. The galaxies in A2646 will have lost most of their gas in the virialization process, which would end most star-formation. A2125 later went on the be one of the galaxies in a sample of 30 rich Abell

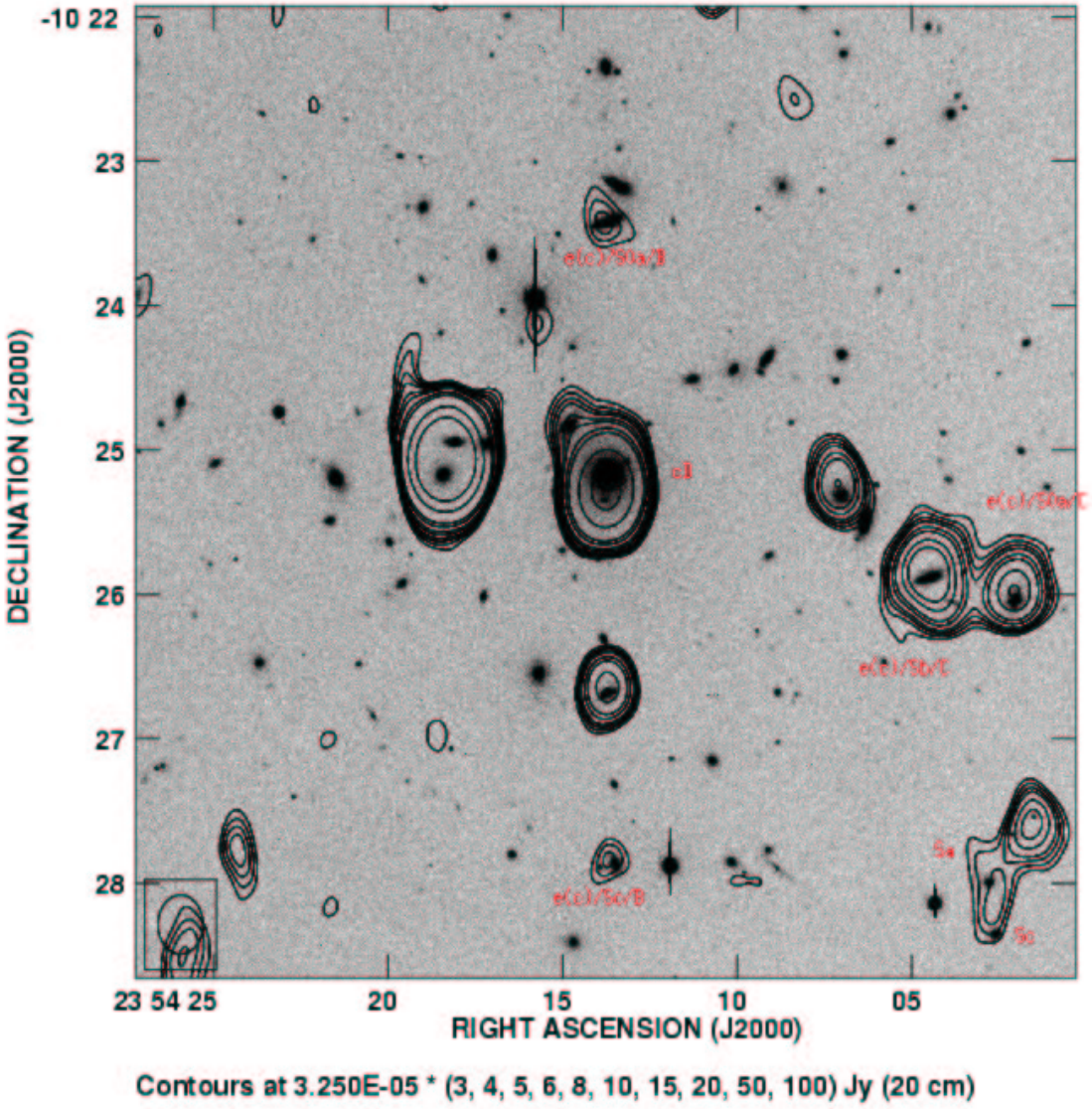

Figure 15: Contourplot of the central 0.6 x 0.6 Mpc centered on the cD galaxy. If known, the spectral type, morphological type and subcluster membership are given for the six SFGs.

clusters at z $\lesssim$ 0.25, reported on by Morrison & Owen in 2003. Even in this large sample they find that A2125 has an exceptionally high number of radio galaxies. Only two other clusters have a relatively high radio galaxy fraction, one of which seems to be a cluster-

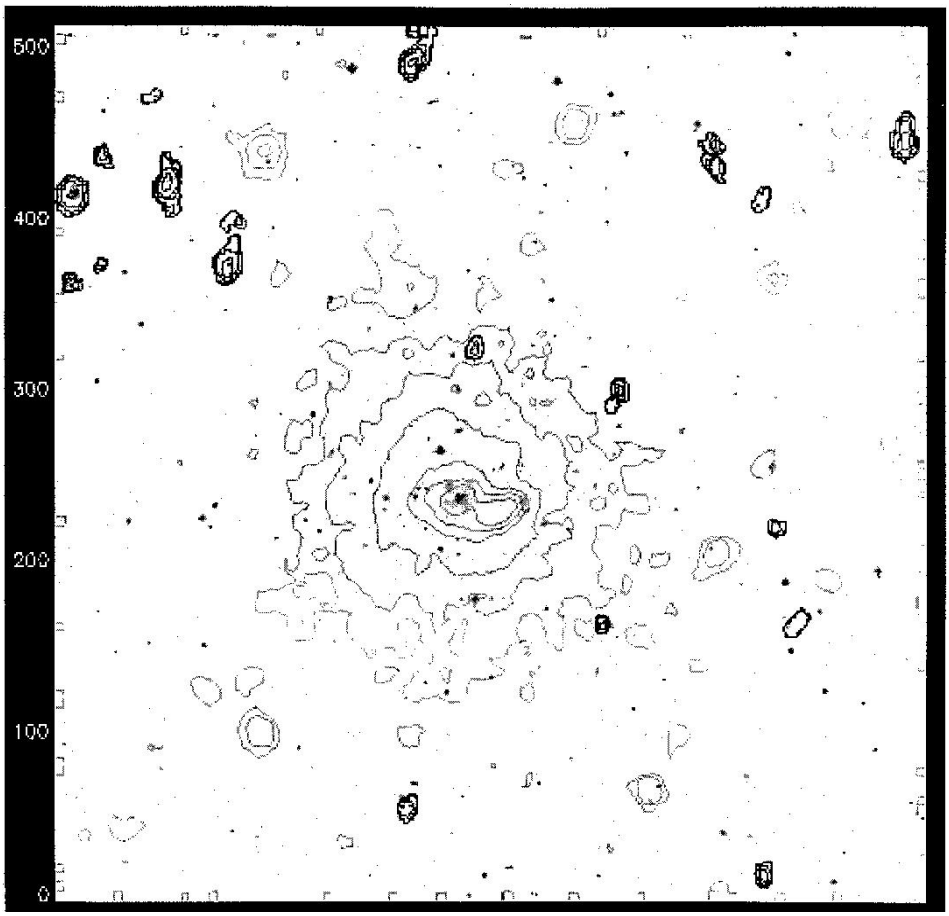

Figure 16: X-ray/HI plot of the center of A2670. Light contours indicate X-ray emission and dark contours HI. The dimensions are roughly 1 Mpc X 1 Mpc. Figure courtesy of van Gorkom.

cluster merger too.

At lower redshift, Miller & Owen (2002) have compared a sample of 20 Abell clusters with each other. 18 of those were of low richness and at a redshift of ~ 0.01 to ~ 0.03 and they were supplemented by Abell 2255 ($z \sim 0.08$, richness class 2) and Abell 2256 ($z \sim 0.06$, richness class 2). All radio observations are comparable, giving lower limit SFRs of 1 $M_\odot$ yr^{-1}. The typical number of radio galaxies found for each cluster is around 20. The only cluster that really jumps out of this sample is Abell 2255, with as much as 46 radio galaxies, 26 of which are star-forming galaxies (although identified as such through their emission lines). The reason for this high activity seems to be once again that subclusters are merging in A2255.

A theory on how star-formation could be enhanced by merging of two clusters is given by Roettiger et al. (1996), who based their results on simulations. According to their theory, a bow shock is created when a small cluster falls into a larger cluster, which protects the galaxies from the infalling cluster from the intra cluster medium and the

galaxies of the larger cluster. When the cluster center gets close, the subcluster galaxies go through the slowed down shock front and due to sudden interaction with the ICM (ram pressure) a number of them will go into a star-bursting phase. This will happen for both the infalling cluster and the primary cluster, and since the shock bow could be Megaparsecs wide, enhancement of star-formation could happen throughout a cluster, not only near the center.

The similarities with A2670 are astonishing. Bird (1994) used the velocity and position data from Sharples et al. to conclude that A2670 consists of three subclusters that are merging along the line of sight. Hobbs & Willmore (1997) use a hierarchical clustering algorithm (for a description they refer to Sokal & Sneath (1973)) to confirm Birds results. Also they remark that observed line-of-sight velocity dispersion profile can not be explained by the mass which they infer from X-ray data. Merging subclusters could do the trick. The morphology of the X-ray (see Figure 16) shows two peaks. The left peak is at the position of the cD galaxy, whereas for the right peak no optical counterpart can be seen. These two peaks do confirm that at least two subclusters are merging. According to Bird, the group of star-forming galaxies to the North-East of the cD galaxy is a subset of one of the three subclusters, subcluster A.

This can be seen in Figure 17, where the positions of the SFGs are plotted again over an outline of the VLA pointings. An A, B or C represents an SFG that is a member of one of the respective subclusters, following Bird. An exclamation mark following an A, B or C indicates the dynamical center of the subcluster. The group of four subcluster A galaxies to the North-West of the center all still contain HI (see figure 16 and Table 2). This could very well mean following Roettigers theory that that group of galaxies just went through the bow shock and is right now heavily interacting with the ICM, resulting in heavy star-formation. That would explain the high number of SFGs in that region, the two subcluster C galaxies found in that area too (that also still contain HI) could be interacting with As bow shock, since according to Bird subcluster C is located at the center of the cluster while A and B are falling in. Possibly, SFGs at other positions throughout the cluster have been triggered by ram pressure after going through their own shock front as well, or the interaction of different bow shocks with galaxies could have caused this. The star-formation ends when due to the ram pressure stripping a galaxy will have lost all its gas.

In any case, the unusual high number of star-forming galaxies can very well be explained by the fact that A2670 is in a state of merging. At higher redshift less clusters are virialized and more clusters will be merging, which means more star-forming galaxies if this theory is correct. Merging of clusters can therefore give at least a partial explanation for the Butcher-Oemler effect.

The eight SFGs in the high density group must have somehow survived the suppression of star-formation that is probably caused by the interaction with the ICM. The interaction with the X-ray may have caused a reboost of star-forming activity, which is supported by the fact that all the high density galaxies are positioned exactly in the X-ray area. The star-bursting galaxy is right at the edge of the X-ray region. Five of them have a very small star-formation rate, which is understandable if they have lost most of their gas due to the ram-pressure stripping, and their activity may soon end.

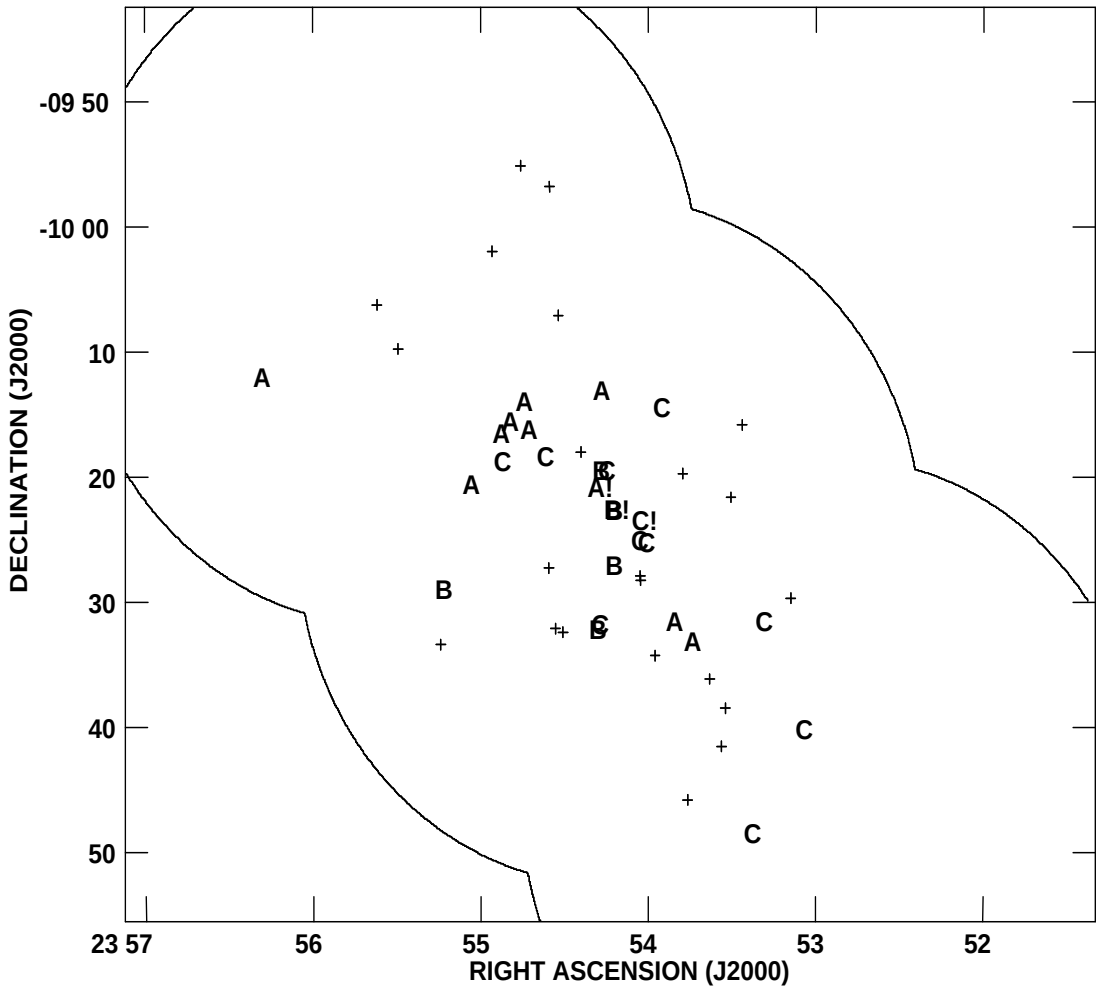

Figure 17: Positions of the radio SFGs plotted on an outline of the VLA pointings. Letters refer to the subclusters the galaxies belong to, following Bird. Letters with an exclamation mark indicate the dynamical centers of the subclusters. Stars indicate SFGs whose subcluster membership is unknown.

The e(c)/S0a galaxy right to the North of the cD galaxy (which is also the galaxy that is closest to the cD galaxy) may be interacting with its Northern neighbour and is also a recent merger of two galaxies, which can be seen by the fact that the galaxy has two nuclei. This may have caused some extra star-formation for that particular case. The two SFGs to the East of the cD galaxy (see Figure 15) have a much higher SFR than one would expect. They are members of the C subcluster, the one that is already forming the center of A2670. They do not have HI left and my prediction is that their star-formation will soon end as they near the cD galaxy any further, although the fact that the galaxy closest to the center of the two has the highest SFR is very suspicious.

5.3 HI

For the star-forming galaxies whose HI content has been detected (HI has been observed down to a mass sensitivity of 10^8 $M_\odot$), a plot of SFR versus HI mass is given in Figure 18. From this plot,no relation can be seen between the HI mass and star-formation rate, the k(e) galaxy with high SFR I have already discussed in section 5.1, it should probably be lower due to contamination from a background source. Clearly the SFGs that were observed in HI are mostly the ones with relatively high SFR. There are two galaxies in the radio sample with such high SFR that you would expect them to have HI observed as well, because their SFR is substantially higher than the average SFR in Figure 18. Those are the star-bursting galaxy at the edge of the X-ray and the westernmost galaxy of the two SFGs right near the center, which I mentioned last section. They have probably lost their HI due to ram-pressure stripping at an earlier stage. The X-ray emission is an obvious candidate to have caused the star-bursting in this phase. According to the Schmidt Law, the SFR can be estimated from the HI mass using a simple equation (Kennicutt 1998):

$$\Sigma_{\rm SFR} = (2.5 \pm 0.7) * 10^{-4} \Sigma_{\rm gas}^{1.4 \pm 0.15} {\rm M}_\odot {\rm yr}^{-1} {\rm kpc}^{-2} \quad (3)$$

with Σ_{gas} the gas surface density in units of $M_\odot$/yr. The red pluses (no e(c) galaxies!) in Figure 19 show the estimated SFRs from galaxies in A2670 in which HI has been detected, where a disk area is used for each galaxy of 750 kpc^2. Most of these predict a SFR too low to be observed in the radio, except for two, one with an HI content of $7.9*10^9$ $M_\odot$ and one of $10.5*10^9$ $M_\odot$. The first one of these was optically detected and classified as an e(b) galaxy. The second one however, was optically not detected at all by Sharples et al. The other way around, the Schmidt Law also provides a way to estimate a possible HI content, when the star-formation rate is known. The X's in Figure 19 indicate the predicted HI mass for the radio SFGs where no HI has been detected. The estimated masses are quite high, but bear in mind that the disk area used of 750 kpc^2 is probably too high for most galaxies, especially since stars are formed only in the inner area of a galaxy. Using a lower disk area the estimated HI masses will shift to the left, so the results given here can be considered to be upper limits. The two galaxies with largest estimated HI mass were mentioned before. More detailed observations will be needed to explain the high activity without HI of these galaxies.

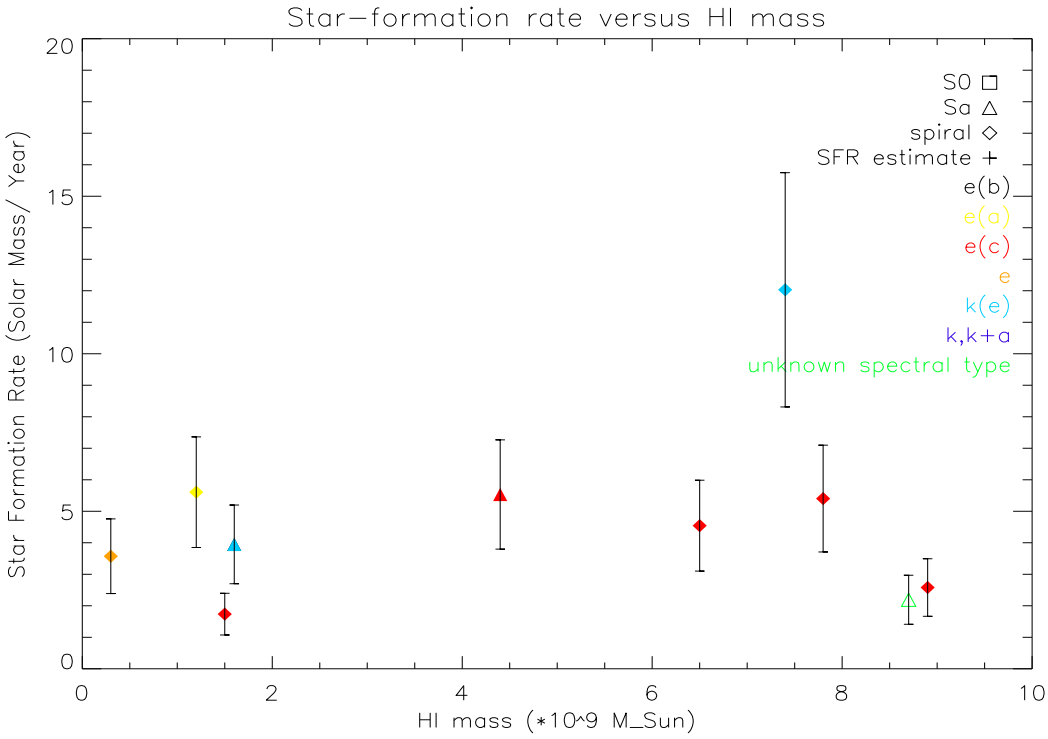

Figure 18: Star-formation rates plotted against HI mass.

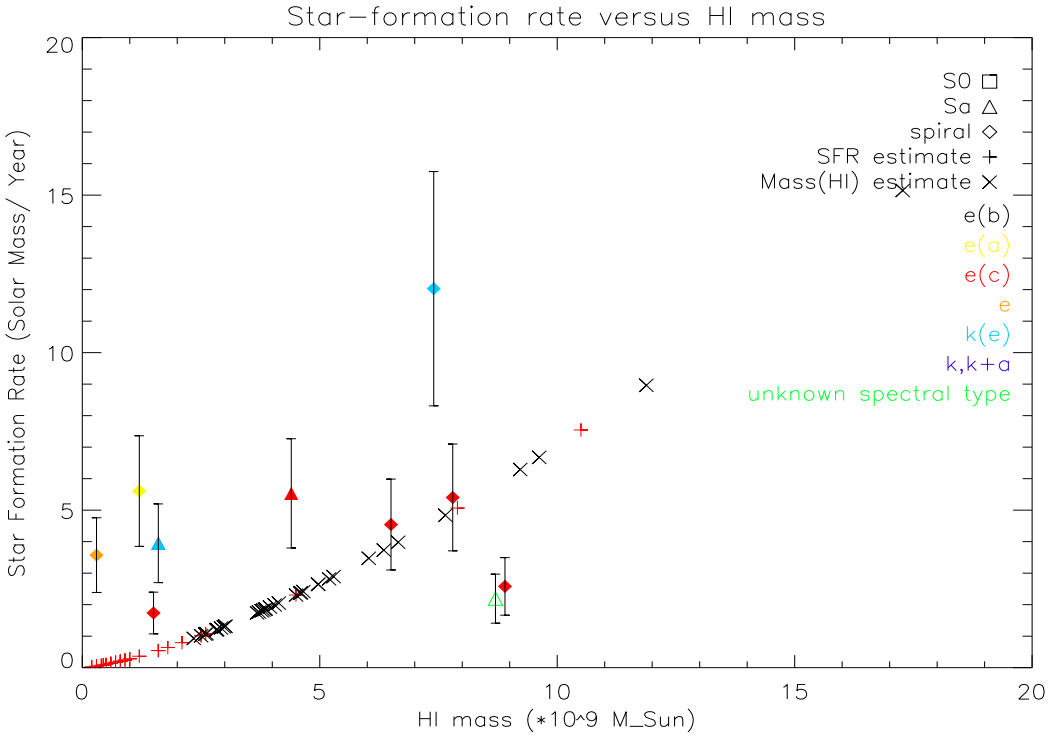

Figure 19: Star-formation rates plotted against HI mass. Red +es (no e(c)'s!) are SFRs estimated from HI mass, X's are HI masses estimated from the SFRs.

6 A comparison with the spectral results

6.1 Comparison of optical and radio samples

When comparing the two populations of SFGs found in the optical and found in the radio, only 20 galaxies are found in both samples (two of which the EW[OII] and hence the optical SFR is not known, so these are not given in Table 3). Only one galaxy found by Sharples et al. fell outside the area observed with the CTIO Schmidt telescope. For the star-forming galaxies that are found by both methods, the ratio of the two star-formation rates is given in Table 3 (SFR_{rad}/SFR_{opt}). The optical SFRs are overall much lower than the radio SFRs. This could be an effect of the chosen method to calculate the SFRs (I refer to Yun, Reddy & Condon (2001) for the radio and to Barbaro & Poggianti (1997) for the optical method of determining the SFR), but the difference in ratios could tell us something about the amount of dust present in the galaxies. The ratios range from about equal (1.2) to as much as 23, with an average of about 7 (the only dusty starburst galaxy (e(a)) in the radio sample has a ratio of 6.1, which is about average). This raises the question whether the equivalent width of the [OII] line has a direct relation with the radio flux, as you would expect if both methods are equally valid. A plot of the normalized radio SFR against EW[OII] for those galaxies that have both can be seen in Figure 20.
Clearly, the e(b) galaxy is classified correctly, both in the optical and in the radio the fluxes are high. Oddly enough however, the galaxy with the highest equivalent width of nearly 60, does not have a very high SFR in the radio. The same goes for the galaxy at $\sim$ 35 Å, of which a higher SFR would also be expected. Moreover, the group on the lower right corner does not show a particularly clear trend toward lower SFR with lower equivalent width, and overall only a marginal relation can be seen between lower EW[OII] and lower SFR. All in all, the relation between EW[OII] and radio SFR seems very unclear judging by this result. This could be the effect of dust-scattering, which gives a lower EW[OII] for equal star-formation rates, making the optical method quite inaccurate. Moreover, SFGs in the radio have been found that were optically classified as passive. That seems to make the optical method even more unreliable. I will come back to this in the next section.
So what about the galaxies in the optical sample that do not have a radio counterpart? The lowest SFR_{rad} to SFR_{opt} ratios in Table 3 are in the order of 1.5. Therefore, it should be possible for optically star-forming galaxies to have a radio SFR comparable to 1.5 times the optical SFR, if we assume that there is not much extinction from dust. If you then compare the expected radio fluxes with the noise levels of the respective region (North-East, center or South-West), six galaxies remain that should have a substantial radio flux that should not be below the $4*\sigma_{noise}$ the radio sample is based on. Those galaxies are given in Table 4. Of all the other optical SFGs not found in the radio a radio flux is expected that is too low to observe at the level I am looking at. In this case therefore the optical method is more sensitive to low star-formation rates.

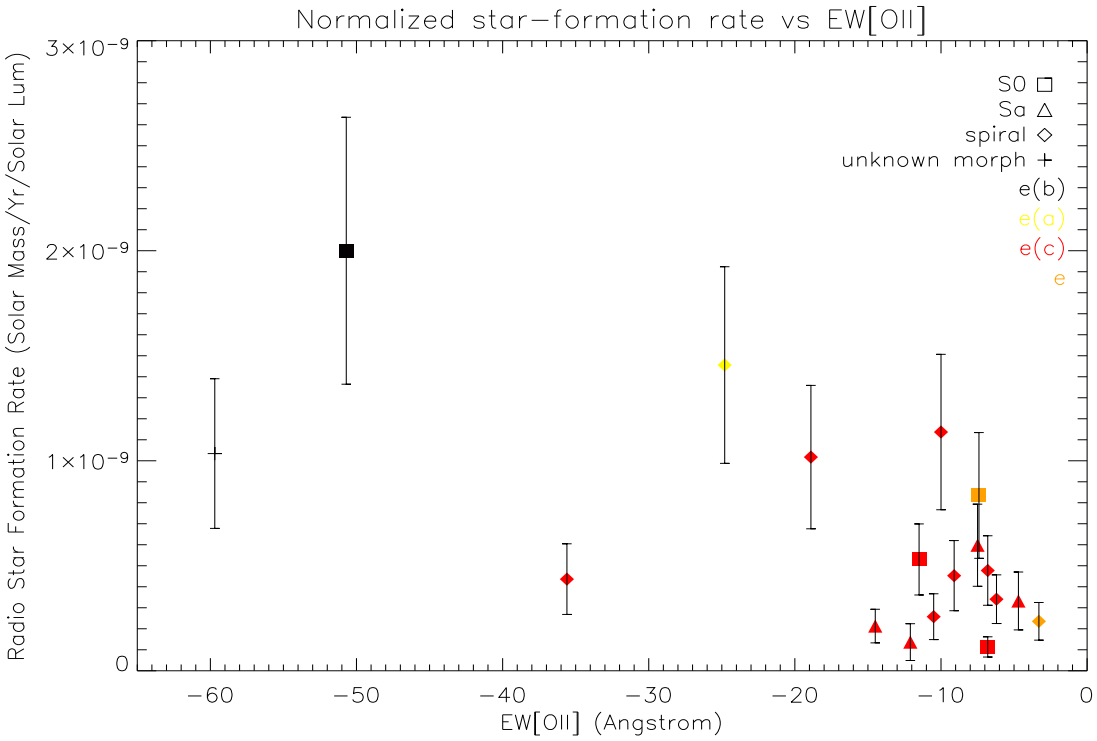

Figure 20: Normalized star-formation rates of radio galaxies whose equivalent width of [OII] is known, plotted against them.

ID #	RA	DEC	SED	sp. type	d(Mpc)	SFR_{opt}	expected S/N
1	23 53 44.01	-10 22 01.3	Inc	e(b)	0.718	2.54 ± 0.56	18
2	23 53 57.20	-10 25 50.2	Sc	e(b)	0.372	0.80 ± 0.20	6
3	23 54 35.79	-09 57 46.4	Sd	e(b)	2.493	1.47 ± 0.32	10
4	23 55 06.03	-10 33 51.7	Sd	e(c)	1.402	0.93 ± 0.21	7
5	23 55 14.18	-10 36 11.4	Inc	e(c)	1.670	0.30 ± 0.07	8
6	23 55 18.00	-09 54 00.2	Sd	e(b)	3.127	1.38 ± 0.33	9

Table 4. Optically strong SFGs without radio counterpart.

The galaxy with ID number 1 has the highest radio flux expectancy. However, as is shown in Figure 21a, not much more than noise can be seen (Note that the contours run from only 1 to 3 times the noise level). The center of the local radio flux is off-centered from the optical galaxy and may just as well come from another source, although the noise is probably responsible for the offset. For numbers 3, 5 and 6 exactly the same can be said, merely radiation which looks like noise is seen, of which a possible center is quite far offset from the center (which may be due to the low S/N). Near galaxies 2 and 4, the galaxies with the lowest expected S/N, not even a possible source can be spotted.

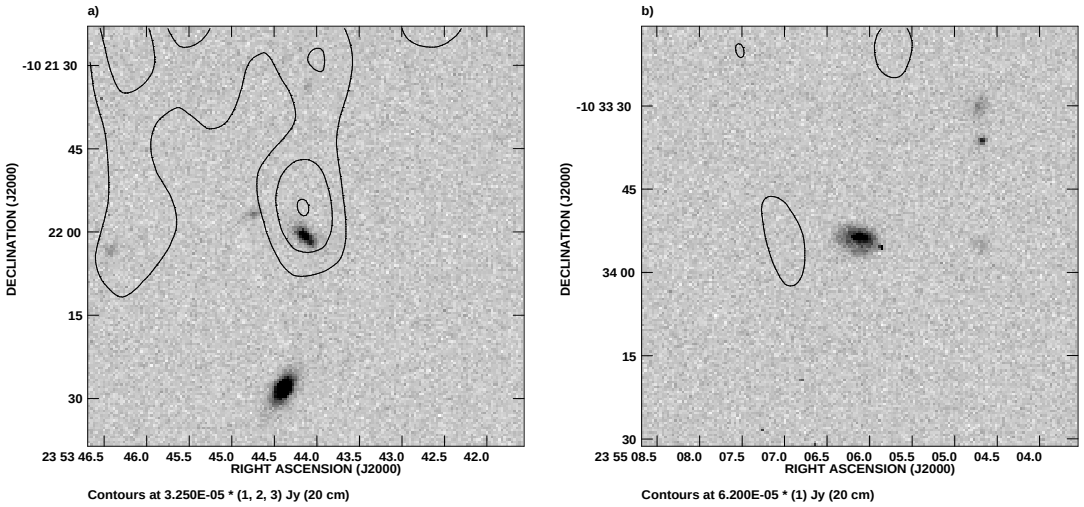

Figure 21: Optical SFGs without radio counterpart. a) Galaxy #1 of Table 4, some flux can be seen, but centered away from the optical image. Note that the contours run from 1 to 3 times the noise-level. b) #4, no radio flux is observed that has anything to do with the galaxy.

Number 4 is shown in Figure 21b. All that can be said is that radio emission can be found near to at least some of these galaxies, but the radio and optical samples are too far off and the radio flux is too low to call it a match.
The spectra of these galaxies definitely show that they are in fact star-forming galaxies. A reason why there is no or hardly any radio flux in these cases, could be that the majority of the stars that have been formed, are still too young to have turned Supernova, which means that no or only little synchrotron emission can be created yet, in any case not representative for the rate of star-formation going on. All the galaxies in Table 4 are very late type and very active galaxies optically, which supports the argument that they have just entered the very active starburst phase. The observation of two galaxies of Figure 20 with high EW[OII] but low radio SFR could be explained by this effect too. This explanation seems very plausible and immediately lays bare the weakness of the method of searching for star-forming galaxies in the radio continuum: before stars have become supernova (which is typically after a few times 10^7 year), the star-formation can not be seen and if only few Supernova explosions have occurred yet the radio flux will not be representative for the star-formation rate. This period is not very long compared to the duration of a typical starburst (typically a few times $\sim 10^8$ year), but not very short either and the effect can clearly be seen in this case. 46 SFGs were observed in the radio and at least six should have been added to this number, which is more than 10%. This is in fact the number you would expect if you compare the lifetime of heavy stars before they go supernova and the lifetime of a starbursting galaxy.

6.2 Optically passive galaxies

In the radio sample, 26 SFGs have not been observed by Sharples et al. at all, because they werent bright enough. Note that all PM galaxies are in the group that is not optically found. Some of them may not be members of A2670 and should in that case be taken out, but the reason that they were classified as PMs in the first place was that they aren't bright enough optically.
Of the galaxies whose spectra is known, one k(e)/Sa galaxy, one k(e)/Sc galaxy, a k:k+a/Sa galaxy and even a k/S0 galaxy are found. They were included in the sample of SFGs on the basis of a low luminosity and a bulge-to-disk ratio that is not convincing enough for the galaxy to be considered an AGN. The k(e)/Sa and the k/S0 galaxy I have mentioned in section 3 (Figure 4b) are probably interacting, judging from the distortion on the lower right corner of the radio flux. Still, because they are not late type spirals it seems like a bit of a stretch to classify them as SFGs, but their low luminosity makes it very improbable that they are both AGNs, coincidentally positioned near to each other. Still, it is quite remarkable that an optically passive galaxy with an S0 morphology should be forming stars. The case of the k(e)/Sc galaxy I have mentioned in section 5 (Figure 8), its radio flux is probably measured higher than it really is due to a background source (moreover, normalized the SFR is not out of line with other galaxies at similar distance/density). In all cases it must be concluded that due to heavy dust the emission got extincted. None of them is located in the high density group, so it is possible ram-pressure stripping hasn't had too much of an effect yet on the dust. Closer observations are needed though to confirm this.
A strong debate has been going on onto whether k+a or a+k galaxies, galaxies that have supposedly recently stopped forming stars, are in fact still forming stars. Smail et al. (1999) detected five galaxies with k+a spectra in the radio continuum in cluster Cl0939+4713. Indeed, using the Hubble Space Telescope large amounts of dust were discovered in those galaxies. Poggianti & Wu (2000) did spectral observations on very luminous infrared galaxies and found that very young stars that are still in the dust cloud they were born in could have their optical emission extincted. Also, Miller & Owen (2001) actively searched for radio detections among 15 post-starburst galaxies and managed to find two cases. Later they found another example in Abell 2255. Finally, Chang et al. 2001 have searched for HI in 5 post-starburst galaxies. They do find some HI in one of the galaxies and find only low upper limits for SFRs, meaning that they do not rule out some remaining star-formation. Still, few examples of k+a galaxies in the radio continuum are known, which is why it is still a controversial subject.
The k+a galaxy I have found in the radio (though it is not even certain to have a k+a spectrum, it is classified as k:k+a which means that it is probably but not certainly a k galaxy. The radio emission seems to indicate that it isnt. The galaxy is located quite far apart from the rest of the SFGs, but its low luminosity and bulge-to-disk ratio definitely seem to indicate that it is not an AGN. Dust obscuration of possibly very young stars must be the cause of the spectral classification. The galaxy just to the West of the starbursting galaxy in Figure 9 is classified as e(c)/k+a(e). Its radio flux is quite low, so in this case it is very possible that the star-formation is on the brink of being truncated,

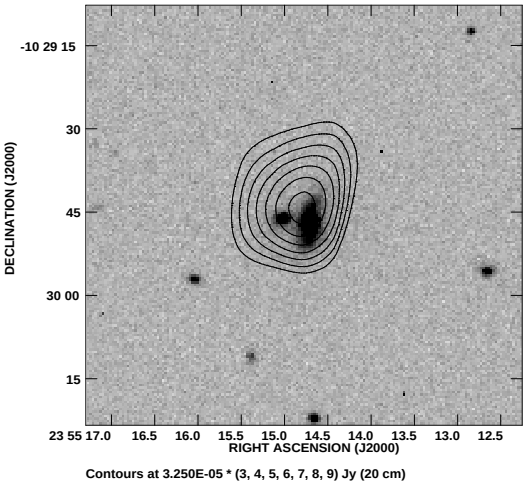

Figure 22: k:k+a galaxy, with Sa morphology.

which explains the observations.
The conclusion seems to be that it is very well possible that galaxies optically classified as more or less passive are still forming stars. Heavy dust obscuration should be responsible for the mis-classification. When [OII] emission is observed then the classification of the galaxy to be star-forming should be taken seriously of course, but the star-formation rate calculated is not reliable and moreover, galaxies without emission lines can not be rejected as star-forming galaxies. The fact that according to Figure 20 the relation between radio SFR and EW[OII] is not clear supports this conclusion.
To see if there is any relation between SFR and optical luminosity, I have plotted the star-formation rates against absolute V magnitude for each SFG from the radio sample in Figure 23 and in Figure 24 for the optical sample. No apparent relation can be seen in either figure.

6.3 Comparison of the optical and radio results

Now let's compare the actual results of the optical sample with the radio sample. As for the "radio" SFGs, I have plotted the positions of the "optical" SFGs on the radio image of A2670 (Figure 25) and also their star-formation rates against distance from the cD galaxy and against galaxy surface density in Figures 26 and 28, with Figures 27 and 29 their respective histograms. Figures 30 and 31 are the same as Figures 26 and 28, but now for normalized SFRs with respect to the V luminosity. The surface density was obtained the same way as it was done for the radio sample, by counting the LM galaxies within a radius of 0.5 Mpc of each SFG.
The optical SFR vs distance plot gives a different picture than the same plot for the radio results. As you can see in figure 27 the number of SFGs seems to increase toward

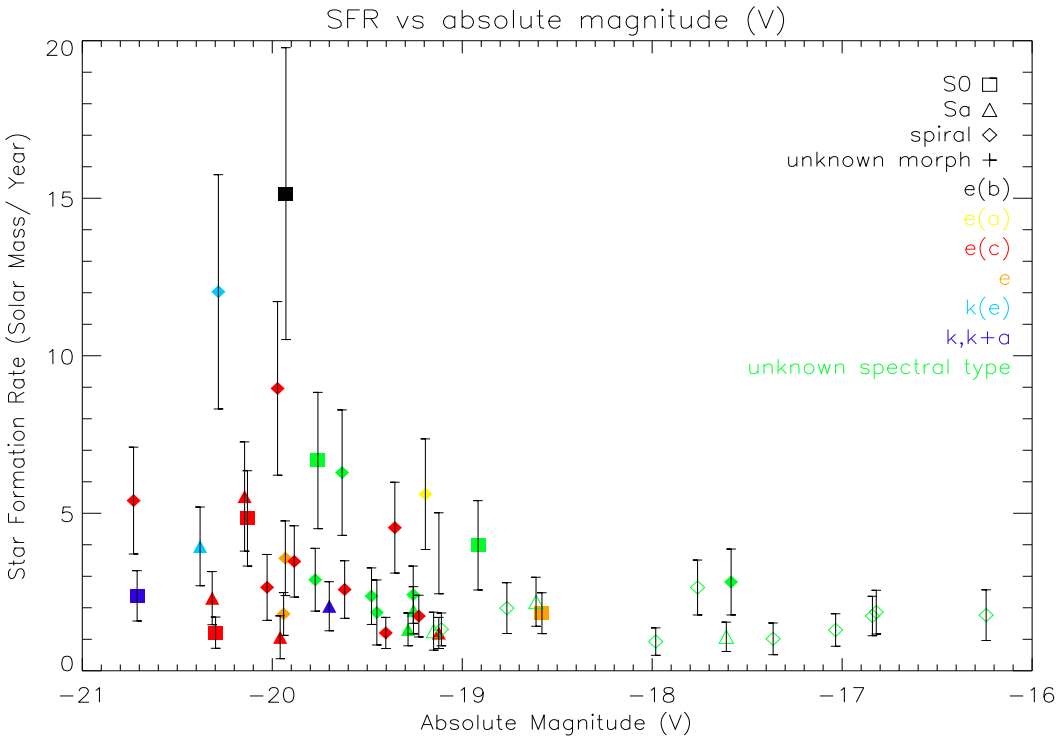

Figure 23: Radio star-formation rates plotted against their optical magnitude in the V band.

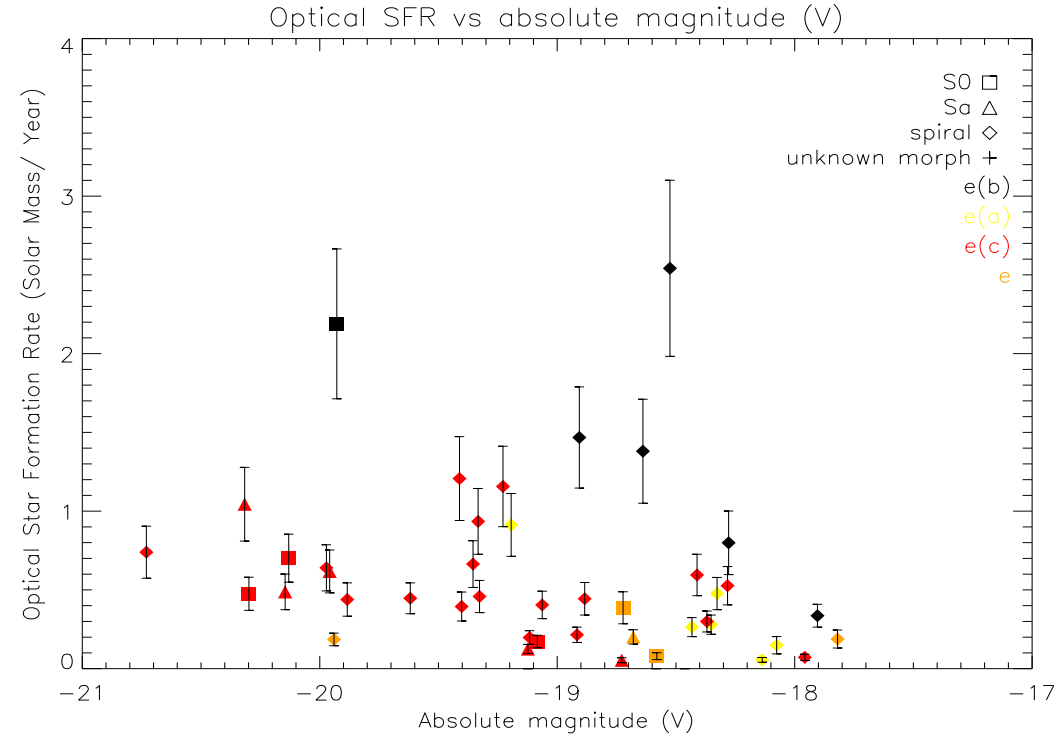

Figure 24: Optical star-formation rates plotted against their optical magnitude in the V band. Of three SFGs from Table 3 the magnitude is not known.

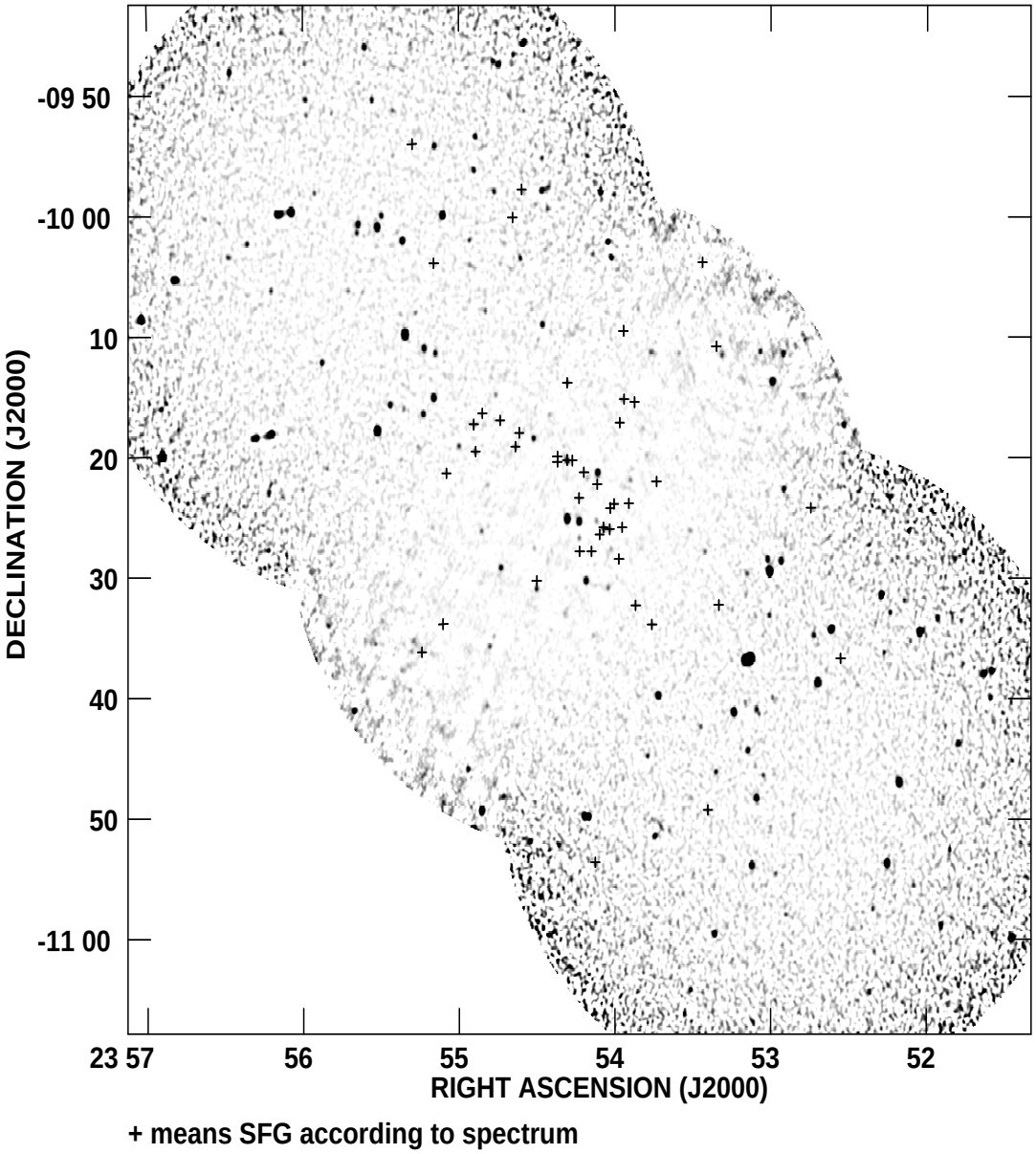

Figure 25: Positions of the optical SFGs plotted on the grey-scale image of the 20 cm radio continuum plot of A2670.

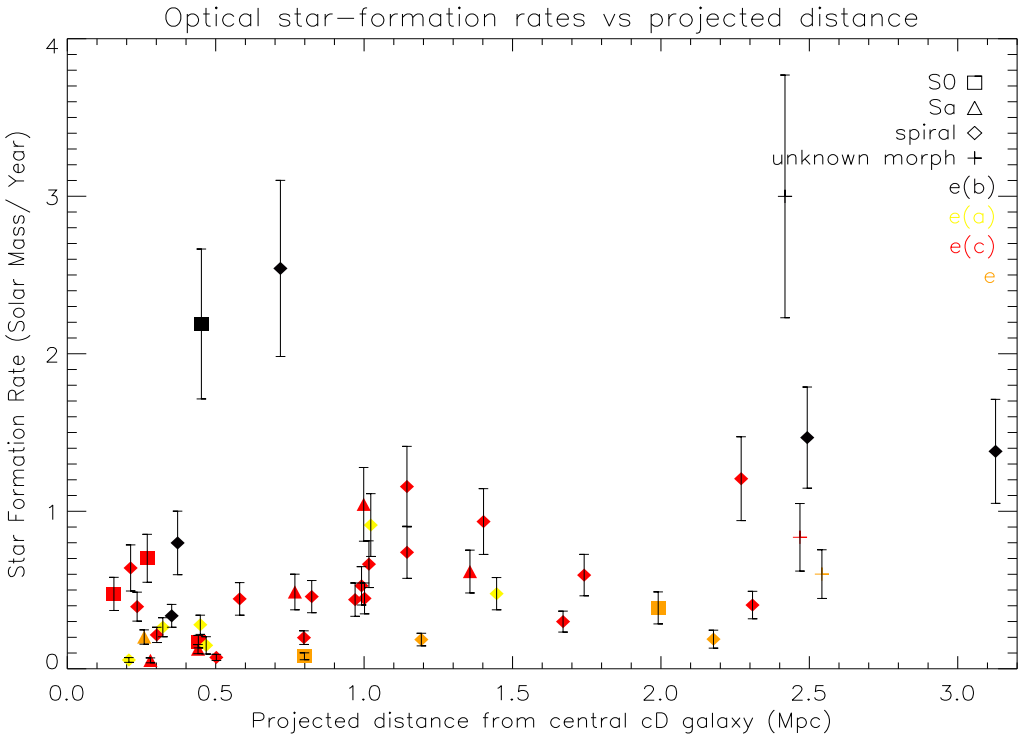

Figure 26: Star-formation rates plotted against projected distance from the cD galaxy. Spectral and morphological types are indicated. Closed symbols are LMs and open symbols are PMs.

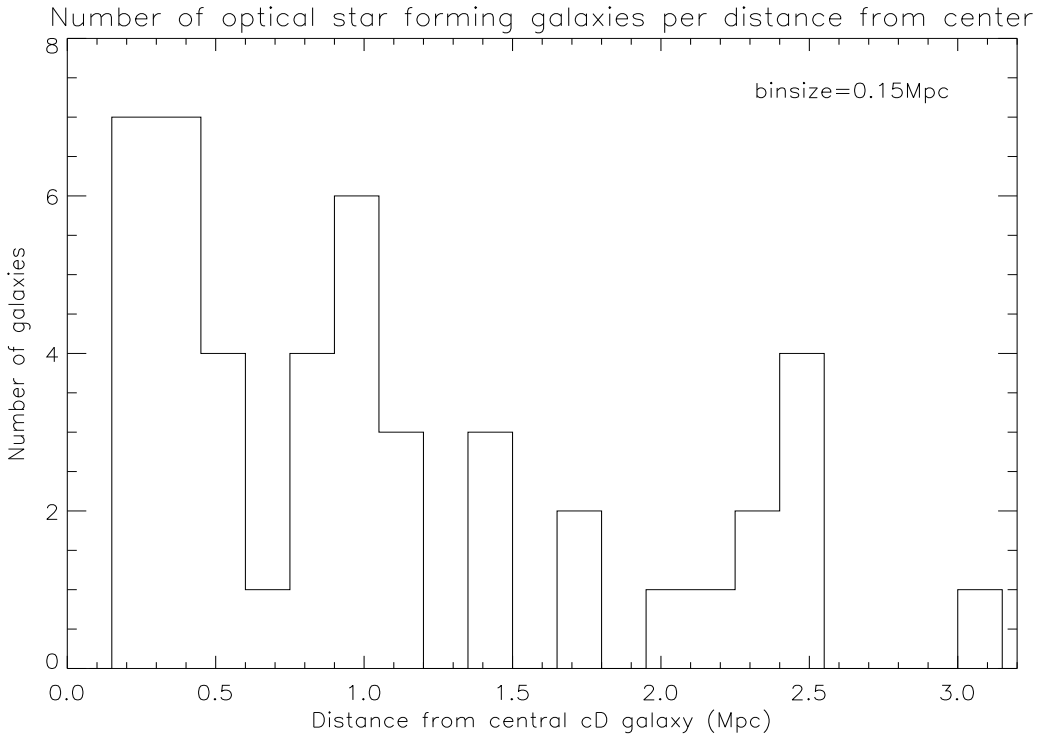

Figure 27: Histogram of the number of optical SFGs per 0.15 Mpc distance from the cD galaxy.

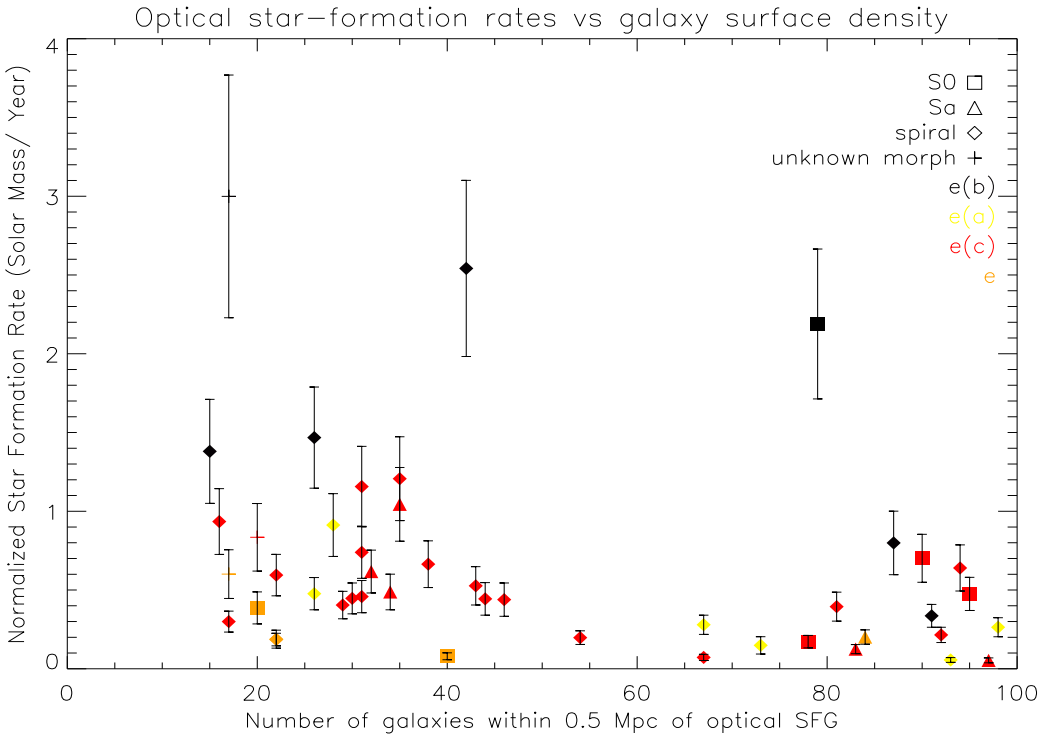

Figure 28: Optical star-formation rates plotted against the number of galaxies in a radius of 0.5 Mpc ($\sim$ an area of 0.8 Mpc^2). Spectral and morphological types are indicated. Closed symbols are LMs and open symbols are PMs. Note: two galaxies were positioned outside the CTIO Schmidt images. For their surface density the values of the nearest SFGs inside the CTIO Schmidt range have been taken.

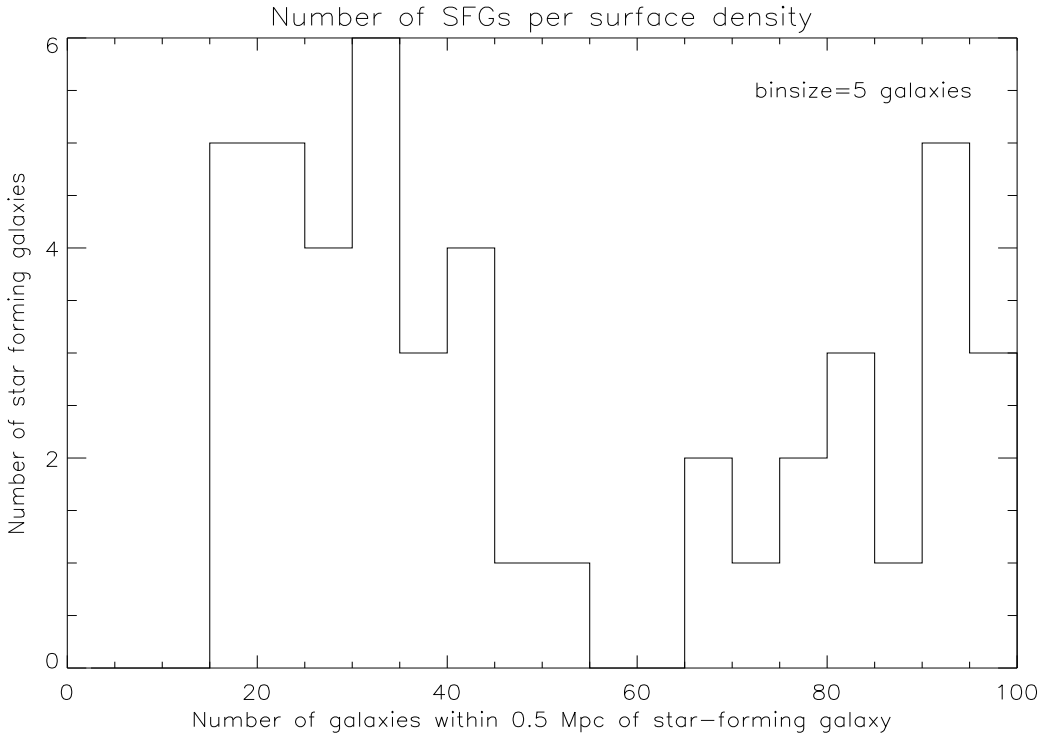

Figure 29: Histogram of the number of SFGs per galaxy surface density.Note: two galaxies were positioned outside the CTIO Schmidt images. For their surface density the values of the nearest SFGs inside the CTIO Schmidt range have been taken.

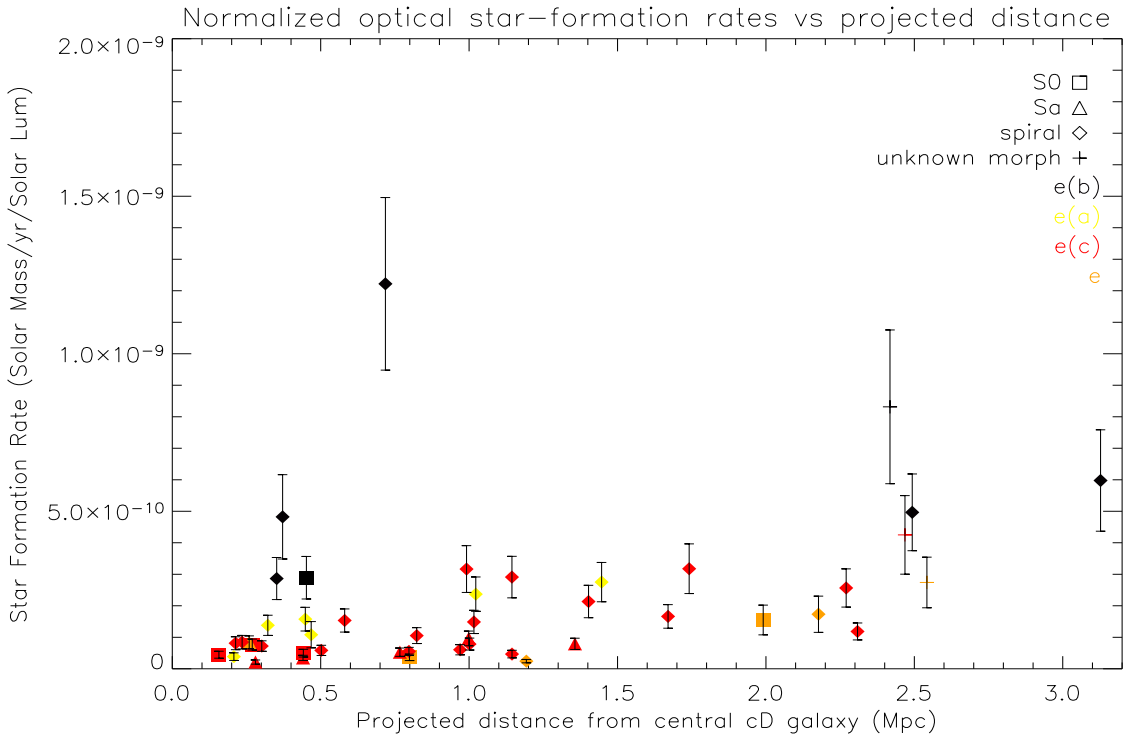

Figure 30: Optical Star-formation rates divided by their V luminosity in terms of solar luminosity, plotted against the distance to the cD galaxy. Spectral and morphological types are indicated. Closed symbols are LMs and open symbols are PMs.

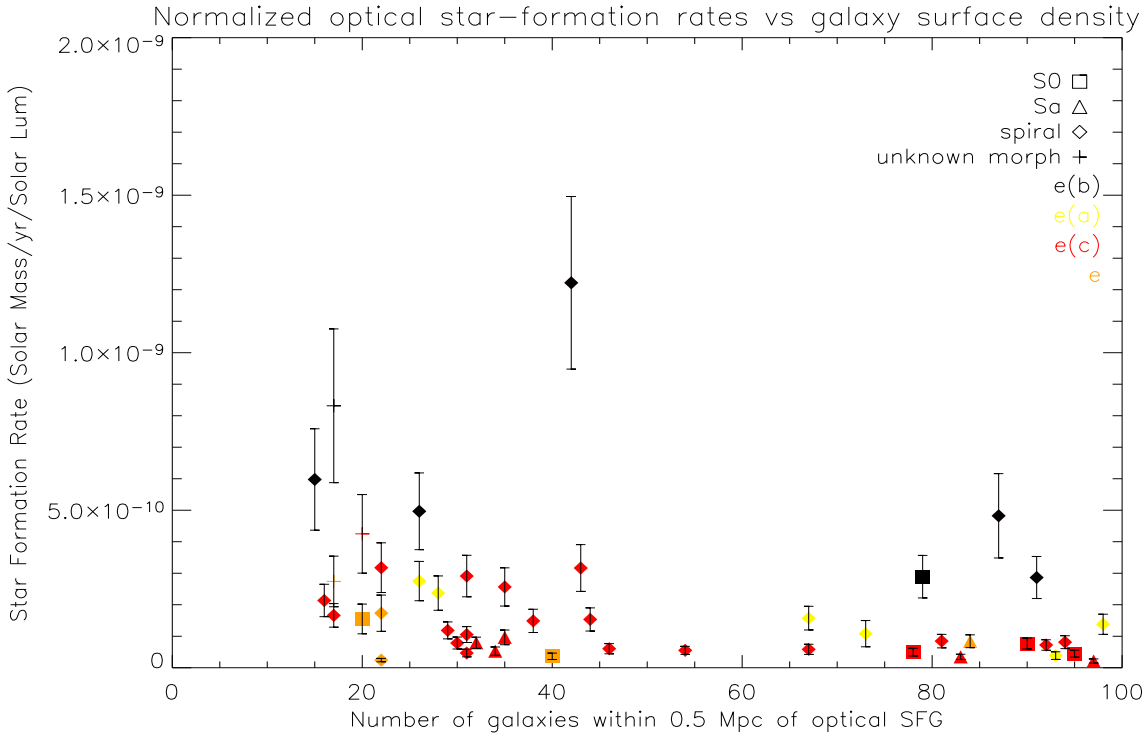

Figure 31: Normalized optical star-formation rates plotted against the number of galaxies in a radius of 0.5 Mpc ($\sim$ an area of 0.8 Mpc^2). Spectral and morphological types are indicated. Closed symbols are LMs and open symbols are PMs. Note: two galaxies were positioned outside the CTIO Schmidt images. For their surface density the values of the nearest SFGs inside the CTIO Schmidt range have been taken.

the center, a peak can be seen near 0.9 Mpc, but closer to the center near $\sim$ 0.3 Mpc an even higher peak is found. Once again though, right near the cD galaxy no SFGs are found, the nearest is found at a distance of $\sim$ 0.15 Mpc, the double nuclei galaxy that was also found in the radio. The density plot once again divides the sample into two groups. A group with density more or less between 15 and 45 and a group with a density more or less between 65 and 100, which is very similar to the optical result, although the high density group has more members in the optical than in the radio. Also once again, the group at hight density completely consists of galaxies lying inside a radius of $\sim$ 0.5 Mpc (the most distant one is at 0.502 Mpc) and the reverse is true too: all found galaxies within that radius can be found in the high density group. In other words, they are the same group, whose galaxies are all located in the X-ray area.
So the main difference between the results of the two methods is that more SFGs are found optically near the center. As explained in the last section this is the result of an optical SFR that gives a radio flux that is too low to be observed in the radio at the level we are looking at. Only galaxies 1 and 2 from Table 4 are close to the center, their star-formation must have begun very recently, so that only few Supernovae could have produced any synchrotron radiation.
Since both samples are incomplete but seem to complete each other, the two samples need to be put together to get a complete picture of the star-formation activity in A2670. Both methods are flawed because they miss galaxies that are forming stars, but the detected SFGs should be taken seriously. Figures 32 and 33 show the histograms of the number of SFGs per distance from the center and per density.
Figure 32 seems to indicate an increasing number of star-forming galaxies toward the center, but what is more telling is that the low-density group in Figure 33 is much larger than the high density group. That means that the majority of the star-forming activity can be explained by the fact that subclusters are merging in A2670. When the subclusters get too close to the center the shock bow will decelerate and the galaxies will cross the border and start interacting with the ICM. Apparently this happens at a density of $\sim$ 20 galaxies per 0.8 Mpc^2. The galaxies in the high-density group are with no exception located in the X-ray region. The interaction with the X-rays must for some galaxies be reason to start forming stars, sometimes even with high star-formation rates.

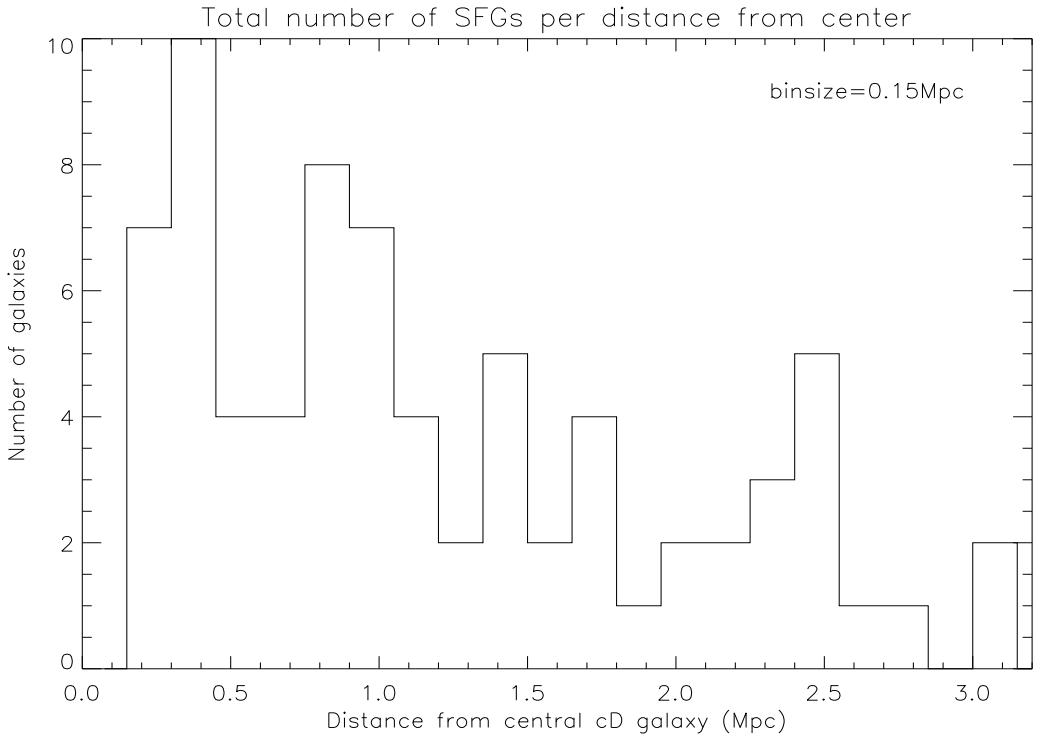

Figure 32: Total number of SFGs with distance from the cD galaxy. The radio and the optical sample are put together.

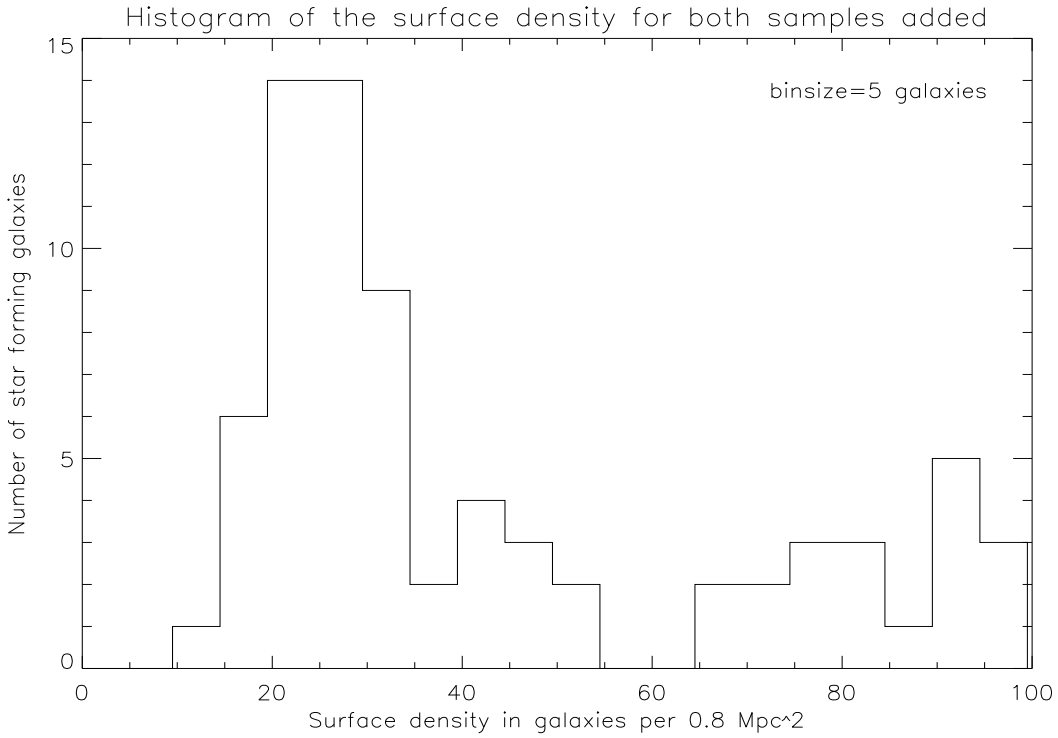

Figure 33: Total number of SFGs with surface density. As before the surface density means the number of LMs within a radius of 0.5 Mpc from each SFG.

7 Conclusions

In Abell 2670 an unusually large amount of star-forming galaxies is present. By comparing images of the 20 cm radio continuum of A2670 with optical images, 46 SFGs were found. The distinguishment between SFGs and AGNs was made primarily by morphology, but also the radio flux, bulge-to-disk ratio, interaction between two galaxies and optical classification were used as criteria. Most of the star-forming galaxies are present near a distance of $\sim$ 0.9 Mpc from the central cD galaxy. However, since the cluster consists of three subclusters that are still merging it is more useful to compare the number and magnitude of the SFGs with their local surface density. Two groups can then be distinguished, one large group at low density (around 30 galaxies per 0.8 Mpc^2) and a smaller group at high density (around 85 galaxies). The low-density group drops in number and activity when moving to higher densities. The high-density group contains a few galaxies with high star-formation rate and a few with low SFR. All the galaxies of the high-density group are positioned inside the X-ray area of A2670, with the outermost one right at the edge.
This high number of star-forming galaxies, may very well be the result of the fact that the cluster is still in a state of merging. Following the model by Roettiger (1996), galaxies that have just crossed the shock bow of their subcluster will be very active due to the sudden and heavy interaction with the ICM they had been protected from earlier. The group of SFGs to the North-East of the center consists mainly of galaxies from one subcluster that still have their HI, so they could very well form an example of galaxies that have just started interacting after passing the shock front. Star-forming galaxies can be found all over the cluster, which might partly be the result of the different shock fronts of the subclusters interacting with galaxies they meet. The high-density group that is forming stars are probably interacting with the X-rays, which encourages them to start forming stars.
The method of detecting SFGs by measuring the flux of the radio continuum however, will not give a complete picture of the star-formation activity. Examining the spectra of $\sim$ 230 galaxies from Abell 2670, 27 galaxies have been classified as star-forming following among others the strength of the [OII] line and the Hδ Balmer line, which were not or not convincingly seen in the radio. Of six galaxies a substantial radio flux would have been expected, yet wasn't observed. The reason for this might well be that these galaxies have started forming stars so recently that no or hardly any stars have gone Supernova yet, which makes it impossible to see the star-formation in the radio. For the other optical SFGs not seen in the radio, a too low radio flux is the cause of no detection. The optical method can therefore be more sensitive when the radio observations do not go deep enough.
The other way round however, four more or less passive galaxies in the optical were found as SFGs in the radio. One of them is an interacting k galaxy and another one is a k+a galaxy. The other two are classified as k(e) galaxies. Heavy dust-obscuration must have been the cause of the false classification, closer observations will be needed to confirm this. Because of these galaxies, plus the fact that the ratio of SFR_{rad} and SFR_{opt} and a plot between radio SFR and EW[OII] give no indication of any relation,

it must be said that the method of optically determining the star-formation activity is very inaccurate. Probably optically found SFGs are in fact forming stars (as of yet there is no reason to believe they aren't), but their star-formation rates are not reliable and SFGs can be overlooked due to heavy extinction.
This means that both methods are not completely reliable and to get a complete picture as possible of the star-formation activity both methods should be used. If that is done for A2670, the theory of the high star-formation activity due to the merging of subclusters is confirmed. The density at which the shock fronts seem to slow down and the galaxies cross them is near $\sim$ 20 galaxies per 0.8 Mpc^2. At higher redshift, more clusters will be in a state of merging. The Butcher-Oemler effect can therefore be at least partially explained by the fact that merging subclusters cause a rise in star-formation activity. The other mechansim responsible for triggering star-formation in Abell 2670 seems to be provided by the X-ray. Very close to the center a group of star-forming galaxies is found both in the optical and in the radio. To of those have an expected HI content that should have been detected, but wasn't. These galaxies will need closer observations in order to determine the process that triggered them to start forming stars.
In the future, more clusters of galaxies at comparable redshift and at higher redshift (both relaxed and not relaxed) will need to be observed to tell if mergers are indeed triggering star-formation. Also, a closer look needs to be taken at X-ray regions in clusters, to see what their effect is on star-forming activity and in what way. To get a better comparison between the optical and radio method of determining the star-forming activity of galaxies, more clusters need to be analyzed using both ways.

Acknowledgements

First of all I would like to thank Jacqueline van Gorkom for inviting me to do this project, and helping me enormously on the way. Also my thanks go out to Mala and Mark, for their great help on various parts of the project and of course their social company.
I wish to thank Bianca Poggianti as well for providing me with all the spectral information, without which a large part of this work could not have been done, and Marc Verheijen for some helpful insights.
Furthermore thanks to all the organisations who have provided me with funding to be able to do this project in New York, and most of all to my father, without whose financial aid this work could never have been done.
Finally, I gratefully acknowledge the support from Hans Rainer Klöckner for putting al his time in setting up AIPS on my computer, which turned out to be not an easy task.

References

Barbaro, G., & Poggianti, B.M. 1997, A&A, 324, 490
Bird, C. 1994, ApJ, 422, 480
Butcher, H., & Oemler, A. 1978, ApJ, 219, 18
Butcher, H. & Oemler, A. 1984, ApJ, 285, 426
Chang, T.Z, van Gorkom, J.H., Zabludoff, A.I., Zaritsky, D, & Mihos, J.C. 2001, AJ, 121, 1965
Condon, J.J. 1992, ARAA, 30, 575
Condon, J.J., Cotton, W.D., & Broderick, J.J. 2002, AJ, 124, 675
Couch, W.J., & Sharples, R.M. 1987, MNRAS, 229, 423
Dressler, A. 1980, ApJ, 236, 351
Dressler, A., & Gunn, J.E. 1983, ApJ, 270, 7
Dressler, A., et al. 1997, ApJ, 490, 577
Dressler, A., et al. 1999, ApJS, 122, 51
Dwarakanath, K.S., & Owen, F.N. 1999, AJ, 118, 625
Hansen, L., et al. 1999, A&A, 349, 406
Hobbs, I.S., & A.P. Willmore 1997, MNRAS, 289, 685
Kennicutt, R.C. 1998, ApJ, 498, 541
Miller, N.A., & Owen, F.N. 2002, AJ, 124, 2453
Miller, N.A., & Owen, F.N. 2003, AJ, 125, 2427
Morrison, G.E., & Owen, F.N. 2003, AJ, 125, 506
Poggianti, B.M., et al. 1999, ApJ, 518, 576
Poggianti, B.M. & van Gorkom, J.H., 2001, ASP Conference Series, Vol. 240 599
Rakos, K.D., & Schombert, J.M. 1995, ApJ, 439, 47
Roettiger, K., Burns, J.O., & Loken, C. 1996, ApJ, 473, 651
Sadler, E.M., et al. 2002, MNRAS, 329, 227
Sage, L.J., & Solomon, P.M. 1989, ApJ, 342, L15
Shambrook, A.A. 2001, PhD thesis, University of California, Santa Cruz
Sharples, R.M., Ellis, R.S., & Gray, P.M. 1988, MNRAS, 231, 479
Smail, I., et al. 1997, ApJS, 110, 213
Smail, I., et al. 1999, ApJ, 525, 609
Sokal, R.A., & Sneath, P.A. 1973, Numerical Taxonomy: The principles and Practice of Numerical Classification, W.H. Freeman and Company, San Francisco
van Gorkom, J.H. 1996, in *Cold Gas at High Redshift, Proceedings of a workshop celebrating the 25th anniversary of the Westerbork Synthesis Radio Telescope*, edited by M.N. Bremer and N. Malcolm, Astrophysics and Space Science Library, Vol. 206, p.145
Yun, M.S., Reddy, N.A., & Condon, J.J. 2001, ApJ, 554, 803